OPTIMAL STRUCTURAL DESIGN FOR MAXIMUM BUCKLING LOAD

by

Yung S. Shin

Dissertation submitted to the Faculty of the

Virginia Polytechnic Institute and State University

in partial fulfillment of the requirements for the degree of

Doctor of Philosophy

in

Civil Engineering

APPROVED:

Raphael T. Haftka, Co-chairman	Raymond H. Plaut, Co-chairman
Richard M. Barker	Siegfried M. Holzer
Kamal Rojiani	Layne T. Watson

August, 1988

Blacksburg, Virginia

OPTIMAL STRUCTURAL DESIGN FOR MAXIMUM BUCKLING LOAD

by

Yung S. Shin

Raphael T. Haftka, Co-chairman

Raymond H. Plaut, Co-chairman

Civil Engineering

(ABSTRACT)

Structural optimization was performed by either mathematical programming methods or optimality criteria methods. Both type of methods are based on iterative resizing of structures in the expectation that it will lead to the satisfaction of optimality conditions. Recent developments in methods for solving nonlinear equations gave a way to an alternative approach in which the optimality conditions are treated as a set of nonlinear equations and solved directly.

Two different formulations are presented; one is a conventional nested approach and the other is a simultaneous analysis and design approach.

Two procedures are explored to solve the nonlinear optimality conditions; a Newton-type iteration method and a homotopy method. Here, the homotopy method is adapted to the optimal design so that we can trace a path of optimum solutions. The solution path has several branches due to changes in the active constraint set and transitions from unimodal to bimodal solutions. The Lagrange multipliers and second-order optimality conditions are used to detect branching points and to switch to the optimum solution path.

This study specifically deals with buckling load maximization which requires highly nonlinear eigenvalue analysis and the procedure is applied to design of a column or laminated composite plate structures. A formulation to obtain mutimodal solutions is given. Also, a special property in a laminate bending stiffness is found. That is, for a given stacking sequence of ply orientations, we showed an existence of a design with the same bending stiffness matrix and same total thickness even when the stacking sequence is changed.

Acknowledgements

This study was supported by the NASA Grant NAG-1-168. This has been greatly appreciated.

I would like to thank the members of my committee for their helpful advise and guidance in this study. I am particularly indebted to my chairmen, Professor Haftka and Professor Plaut, for their encouragement and timely suggestions.

I also wish to thank my office-mates at Femoyer for their friendship and support.

Special thanks is due to my wife, Mi-Ae. Without her support and encouragement, this work would not have been possible.

Finally a very special acknowledgement must be awarded to my parents, Mrs. Yun-Sik Kim Shin and Mr. Yun-Chin Shin. Their love, faith, and support were so necessary in achieving this goal.

Table of Contents

List of Illustrations

List of Tables

Chapter 1

Introduction

Structural optimization has gained popularity in recent years as the importance of minimum weight design has been recognized in many industries such as the aerospace or the automotive industries. Conventionally, structural optimization is performed by either mathematical programming methods or optimality criteria methods. Both type of methods are based on iterative resizing of structures in the expectation that it will lead to the satisfaction of optimality conditions. The optimality conditions can be obtained from variational formulation of the design problem. However, mathematical programming methods do not pose the optimality conditions, rather, they employ standard minimization techniques to reach an optimal design. Optimality criteria methods pose the optimality conditions, however, they seek indirect methods to solve them.

An alternative approach is to treat the optimality conditions as a set of nonlinear equations and to solve them directly. This approach was not popular in the past because of the shortcoming of available procedures for solving nonlinear algebraic equations. However, recent developments in methods for solving nonlinear equations [1] are prompting a reassessment of this alternative.

The present study explores two different formulations of direct solution of optimality conditions. One is a conventional nested approach where only the structural parameters are unknown. The other is a simultaneous analysis and design approach where both response and structural dimensions are design variables. The simultaneous approach was initiated by Schmit and his co-workers [2-4] in an attempt to integrate equations for structural analysis and optimum design. Recent papers by Haftka and Kamat [5, 6] report computational advantages for the simultaneous approach over the nested approach when applied to nonlinear structural problems. They used a preconditioned conjugate gradient method [7] and the element by element (EBE) formulation of Hughes et al. [8].

Two procedures are explored to solve the nonlinear optimality conditions. One is a Newton-type iteration method and the other is a homotopy method. First, we start with a Newton-type method. One of the difficulties with a solution of optimality conditions is that there are many nonoptimal solutions due to highly nonlinear nature of optimality equations, so that the correct solution must be identified. The use of second-order conditions is explored to validate solutions obtained from the first-order optimality conditions. Another difficulty in using a Newton-type method is that the method is not guaranteed to converge to the solution, unless the initial estimate is very close to it. A tracing technique is developed to eliminate this difficulty. The tracing technique employs a homotopy method to trace the optimal solution with guaranteed convergence.

The basic theory of globally convergent (convergent from an arbitrary starting point) homotopy methods was developed in 1976[9, 10]. Since then, the method has been used in a wide range of scientific and engineering problems. It has been successfully applied to nonlinear complementarity problems [11], nonlinear two-point boundary value problems [12], fluid dynamics problems [13, 14] and nonlinear elastica problems [15, 16]. References [17, 18] show the application to optimum structural design problems discretized by plane stress finite elements. Reference [17] shows that an appropriate homotopy method is globally convergent for an optimum design problem. In the present study, the original globally convergent homotopy method is adapted to the optimal structural design. The study shows how the solution process can start from the minimum amount of resources which is required for a feasible solution to the highest value that may be of interest. This yields a bonus in that we get an entire family of optima parameterized by the amount of resources.

This study specifically deals with buckling load maximization which requires highly nonlinear eigenvalue analysis and the procedure is applied to design of a column or laminated composite plate structures.

Chapter 2 presents the formulation for the simultaneous analysis and design approach for a general eigenvalue constraint. These problems often have bimodal solutions, that is, the optimum eigenvalue has two eigenvectors associated with it [19]. Thus, a bimodal formulation of the optimization is also given. This approach is applied to two problems: optimum column design with a given foundation and optimum design of the foundation for a given column.

In Chapter 3, the strategy for tracing a path of optimum solutions is given. Equations for the optimum path are obtained using Lagrange multipliers, and solved by the homotopy method. The solution path has several branches due to changes in the active constraint set and transitions from unimodal to bimodal solutions. The Lagrange multipliers and second-order optimality conditions are used to detect branching points and to switch to the optimum solution path. The procedure is applied to the design of a foundation which supports a column for maximum buckling load. Using the total available foundation stiffness as a homotopy parameter, a set of optimum foundation designs is obtained.

Chapter 4 and Chapter 5 deal with the design of laminated composite plates subject to buckling loads. In Chapter 4, it is shown that for any design with a given stacking sequence of ply orientations, there exists a design associated with any other stacking sequence which possesses the same bending stiffness matrix and same total thickness. Hence, from the optimum design for a given stacking sequence, one can directly determine the optimum design for any rearrangement of the ply orientations, and the optimum buckling load is independent of the stacking sequence.

In Chapter 5, the buckling load of laminated plates having midplane symmetry is maximized for a given total thickness. The thicknesses of the layers are taken as the design variables. The optimality equations are solved by a homotopy method so that we can trace all the optima as a function of total volume of the plate. In Chapter 3, the homotopy optimization method was formulated using a simultaneous approach; here, the same method is applied with the more traditional sequential approach in which the buckling analysis is performed repeatedly. Buckling analysis is carried out using the finite element method. Two examples are presented; the design of unstiffened laminated plates and the design of stiffened laminated plates.

Chapter 2

Simultaneous Analysis and Design Approach

One objective of this chapter is to formulate the simultaneous analysis and design approach for eigenvalue maximization. The formulation leads to a set of non-linear algebraic equations for the discretized structure. Both unimodal and bimodal optimum solutions are considered. The second objective is to apply the simultaneous formulation to the optimum design of beam-columns with elastic foundations.

There has been a number of studies on the optimum design of structures with given foundations and eigenvalue constraints. Vibrating beams with frequency constraints were considered in Refs. [20] and [21], and columns with buckling load constraints were considered in Refs. [19] and [22-24]. In Ref. [19], Kiusalaas presented an example of a simply supported column on a given foundation. He showed that the optimal solution could be bimodal, i.e., the lowest buckling load could be a repeated eigenvalue. This problem has recently been studied in more detail by Gajewski [23] and Plaut, Johnson, and Olhoff [24]. In Ref. [24] it was shown that bimodal solutions appear in certain ranges of foundation stiffness for columns with various boundary conditions.

The optimum distribution of foundation stiffness for given structures subject to eigenvalue constraints was only studied in Ref. [25]. The minimum natural frequency of a vibrating beam was maximized. Under special conditions, the optimal solution is bimodal.

2.1 Formulation

2.1.1 Optimization Problem

The smallest eigenvalue P of a vibration or buckling problem can be expressed by Rayleigh's quotient:

$$P = \min_{y} \frac{V(d,y)}{L(d,y)} \tag{2-1}$$

where d is a structural material distribution function, y is the displacement function, V(d,y) is the elastic energy functional and L(d,y) is a kinetic energy functional (for the vibration problem) or a work functional (for the buckling problem).

The design problem we consider here is to maximize P for a given amount of resources with some subsidiary constraints on d (such as upper or lower limits). This problem is written as

$$\max_{d} \; \min_{y} \; \frac{V(d,y)}{L(d,y)} \tag{2-2}$$

$$\text{such that } \; H(d) = 0$$

$$g(x,d) \geq 0$$

where the functional H(d) represents a resource constraint, x is the coordinate vector, and g(x,d) is the subsidiary constraint.

The functionals V(d,y) and L(d,y) are homogeneous functionals of the same order, and so, instead of the problem (2-2), it is permissible to require L(d,y) = 1 and form the following Lagrangian function:

$$P^* = V(d,y) - \eta\{L(d,y) - 1\} - \mu H(d) - \int_X \Lambda(x)\,\{g(x,d) - T^2(x)\}dx \qquad (2-3)$$

where η and μ are Lagrange multipliers, Λ is a Lagrange-multiplier function, and T is a slack variable function.

Next, the unknown functions d, y, Λ, and T are discretized in space as

$$\begin{aligned} d &= \sum_{i=1}^{M} a_i\,\overline{d}_i(x) \\ y &= \sum_{i=1}^{N} b_i\,\overline{y}_i(x) \\ \Lambda &= \sum_{i=1}^{P} \lambda_i\,\overline{\Lambda}_i(x) \\ T &= \sum_{i=1}^{Q} t_i\,\overline{T}_i(x) \end{aligned} \qquad (2-4)$$

Also, a_i is replaced by β_i^2 to prevent the material distribution function d from having negative values. Substituting from equations (2-4) into equation (2-3), P* becomes a function of the unknown scalar quantities β_i, b_i, λ_i, t_i, μ, and η.

2.1.2 First-Order Conditions

The necessary conditions for an optimum are obtained by taking the first derivatives of P* with respect to β_i, b_i, λ_i, t_i, μ, and η and setting them to zero. Thus we obtain

i) Optimality conditions

$$\frac{\partial V(d,y)}{\partial \beta_i} - \eta \frac{\partial L(d,y)}{\partial \beta_i} - \mu \frac{\partial H(d)}{\partial \beta_i} - \int_x \Lambda(x) \frac{\partial g(x,d)}{\partial \beta_i}\, dx = 0 \qquad \text{for } i = 1, \ldots, M \qquad (2-5)$$

ii) Stability conditions

$$\frac{\partial V(d,y)}{\partial b_i} - \eta \frac{\partial L(d,y)}{\partial b_i} = 0 \qquad \text{for } i = 1, \ldots, N \qquad (2-6)$$

iii) Local inequality constraints (1)

$$\int_x \{g(x,d) - T^2(x)\}\, \overline{\Lambda}_i(x)\, dx = 0 \qquad \text{for } i = 1, \ldots, P \qquad (2-7)$$

iv) Local inequality constraints (2)

$$\int_x \Lambda(x)\, T(x)\, \overline{T}_i(x)\, dx = 0 \qquad \text{for } i = 1, \ldots, Q \qquad (2-8)$$

v) Resource constraint

$$H(d) = 0 \qquad (2-9)$$

vi) Normalization constraint

$$L(d,y) = 1 \qquad (2-10)$$

Equations (2-5)-(2-10) are non-linear simultaneous equations with unknowns β_i, b_i, λ_i, t_i, μ, and η. After these equations are solved numerically, the optimum material distribution, d, and the displacement field, y, are obtained from equations (2-4).

2.1.3 Check for Optimality

The first derivatives provide only a necessary condition for the optimum design, and there may be multiple solutions to these non-linear equations. The true optimum solution must then be determined from these multiple solutions.

First, we need to check the Kuhn-Tucker conditions:

$$\lambda_i \geq 0 \qquad \text{for } i = 1, \ 2, \dots , P \qquad (2-11)$$

Then, the second-order optimality conditions should be checked. The second-order conditions are given in Ref. [26] for a minimization problem. Our optimum design problem is a min-max problem in which the objective function, P^*, is maximized with respect to the material distribution variables, β_i , and minimized with respect to the displacement field variables, b_i.

The second-order necessary conditions for optimality are

$$\begin{aligned} & r_1^T \, [\nabla_\beta^2 P^*] \, r_1 < 0 \qquad \text{for every } r_1 \text{ such that} \\ & \qquad \nabla_\beta \, h_p^T \, r_1 = 0 \qquad \text{for} \quad p = 1, \ 2 \qquad (2-12) \\ & \qquad \nabla_\beta \, g_m^T \, r_1 = 0 \qquad \text{for} \quad m = 1, \ 2, \dots , P \qquad \text{for those constraints with } \lambda_m > 0 \end{aligned}$$

where $[\nabla_\beta^2 P*] = \left[\frac{\partial^2 P*}{\partial \beta_i \, \partial \beta_j} \right]$ for $i = 1, \dots, M$ and $j = 1, \dots, M$

$$h_1 = H(d)$$

$$h_2 = L(d,y) - 1$$

$$g_m = \int_x \{g(x,d) - T^2(x)\} \, \overline{\Lambda}_m(x) \, dx$$

and

$$r_2^T \, [\nabla_b^2 P*] \, r_2 > 0 \qquad \text{for every } r_2 \text{ such that} \qquad \nabla_b h_2^T \, r_2 = 0 \tag{2 – 13}$$

where $[\nabla_b^2 P*] = \left[\frac{\partial^2 P*}{\partial b_s \, \partial b_t} \right]$ for $s = 1, \dots, N$ and $t = 1, \dots, N$

2.1.4 Bimodal Formulation

The above formulation only gives unimodal solutions (i.e., solutions which have a single eigenvector associated with the eigenvalue). To seek the solutions with double eigenvectors, the problem is to be formulated assuming bimodality of solutions, or equality of the two lowest eigenvalues, P_1 and P_2. They are expressed in terms of the Rayleigh quotient:

$$P_i = \frac{V(d,y_i)}{L(d,y_i)} \qquad \text{for } i = 1, \; 2 \tag{2 – 14}$$

where y_i are the corresponding eigenvectors.

Treating the bimodality condition as an equality constraint, $P_1 - P_2 = 0$, the augmented functional $P*$ is formed:

$$P^* = V(d,y_1) - \gamma\{V(d,y_1) - V(d,y_2)\} - \sum_{i=1}^{2}\eta_i\{L(d,y_i) - 1\} - \mu H(d) - \int_x \Lambda(x)\{g(x,d) - T^2(x)\}dx \qquad (2-15)$$

The eigenvectors y_1 and y_2 need to be distinct, and this could be accomplished by including an orthogonality constraint in equation (2-15). However, in this paper it is accomplished by the discretization procedure. Discretization for y in equations (2-4) is replaced by

$$y_1 = \sum_{i=1}^{N/2} b_i\bar{y}_{1i}(x)$$
$$y_2 = \sum_{i=1}^{N/2} c_i\bar{y}_{2i}(x). \qquad (2-16)$$

The first-order conditions, equations (2-5) - (2-10), are replaced by

i) Optimality conditions

$$\frac{\partial V(d,y_1)}{\partial \beta_i} - \gamma\{\frac{\partial V(d,y_1)}{\partial \beta_i} - \frac{\partial V(d,y_2)}{\partial \beta_i}\} - \sum_{j=1}^{2}\eta_j\frac{\partial L(d,y)}{\partial \beta_i} - \mu\frac{\partial H(d)}{\partial \beta_i} - \int_x \Lambda\frac{\partial g(x,d)}{\partial \beta_i}\,dx = 0 \qquad (2-17)$$

for $i = 1, \dots, M$

ii) Stability conditions

$$(1-\gamma)\frac{\partial V(d,y_1)}{\partial b_i} - \eta_1\frac{\partial L(d,y_1)}{\partial b_i} = 0 \qquad \text{for } i = 1, \dots, N/2 \qquad (2-18a)$$

$$\gamma\frac{\partial V(d,y_2)}{\partial c_i} - \eta_2\frac{\partial L(d,y_2)}{\partial c_i} = 0 \qquad \text{for } i = 1, \dots, N/2 \qquad (2-18b)$$

iii) Local inequality constraints (1)

$$\int_x \{g(x,d) - T^2(x)\}\,\overline{\Lambda}_i(x)\,dx = 0 \qquad \text{for } i = 1, \dots, P \tag{2-19}$$

iv) Local inequality constraints (2)

$$\int_x \Lambda(x)\,T(x)\,\overline{T}_i(x)\,dx = 0 \qquad \text{for } i = 1, \dots, Q \tag{2-20}$$

v) Bimodality constraint

$$V(d,y_1) - V(d,y_2) = 0 \tag{2-21}$$

vi) Resource constraint

$$H(d) = 0 \tag{2-22}$$

vii) Normalization constraints

$$L(d,y_i) = 1 \qquad \text{for} \quad i = 1,\ 2 \tag{2-23}$$

A new notation e_i is introduced as variables which comprise b_j and c_j,

$$e_i = \{b_1,\ b_2, \dots, b_{N/2}, c_1,\ c_2, \dots, c_{N/2}\}^T \qquad \text{for } i = 1, \dots, N \tag{2-24}$$

Then the second-order conditions (equations (2-12) and (2-13)) are replaced by

$$r_1^T\,[\nabla_\beta^2 P^*]\,r_1 < 0 \qquad \text{for every } r_1 \text{ such that}$$

$$\begin{aligned} &\nabla_\beta h_p^T r_1 = 0 \qquad \text{for} \quad p = 1, \dots, 4 \\ &\nabla_\beta g_m^T r_1 = 0 \qquad \text{for} \quad m = 1,\ 2, \dots, P \qquad \text{for those constraints with } \lambda_m > 0 \end{aligned} \tag{2-25}$$

where $[\nabla_\beta^2 P^*] = \left[\dfrac{\partial^2 P^*}{\partial \beta_i\, \partial \beta_j} \right]$ for $i = 1, \dots, M$ and $j = 1, \dots, M$

$$\begin{aligned} h_1 &= V(d,y_1) - V(d,y_2) \\ h_2 &= H(d) \\ h_3 &= L(d,y_1) - 1 \\ h_4 &= L(d,y_2) - 1 \\ g_m &= \int_x \{g(x,d) - T^2(x)\}\, \overline{\Lambda}_m(x)\, dx \end{aligned}$$

and

$$r_2^T\,[\nabla_e^2 P^*]\,r_2 > 0 \qquad \text{for every } r_2 \text{ such that}$$

$$\nabla_e h_p^T r_2 = 0 \qquad \text{for} \quad p = 1,\ 2,\ 3 \tag{2-26}$$

where $[\nabla_e^2 P^*] = \left[\dfrac{\partial^2 P^*}{\partial e_s\, \partial e_t} \right]$ for $s = 1, \dots, N$ and $t = 1, \dots, N$

$$\begin{aligned} h_1 &= V(d,y_1) - V(d,y_2) \\ h_2 &= L(d,y_1) - 1 \\ h_3 &= L(d,y_2) - 1 \end{aligned}$$

2.1.5 Computer Implementation

Since the method described above requires the solution of a large system of non-linear equations, a systematic solution process was adopted to obviate the need for an exhaustive search through the multiple solutions. The overall solution process is as follows:

a. Start with small numbers for M, the number of material variables, and N, the number of response variables.

b. Select uniform initial values for material variables and the corresponding first or second eigenvector as initial values for the response variables.

c. Obtain the solution of the first derivative equations.

d. Check the Kuhn-Tucker conditions and the second-order conditions. If satisfied, double the number of variables, M and N. If not, choose new initial values of β_i and b_i(or e_i), and go to step c.

e. Stop when M is large enough to approximate a smooth material distribution.

For solving these nonlinear systems of equations (equations (2-5)-(2-10) or (2-17)-(2-23)), an IMSL routine, ZSPOW, is used. ZSPOW is based on the MINPACK subroutine HYBRD1, which uses a modification of M.J.D. Powell's hybrid algorithm [27]. This algorithm is a variation of Newton's method which uses a finite-difference approximation to the Jacobian and takes precautions to avoid large step sizes or increasing residuals.

2.2 Optimal Column on Elastic Foundation Example

2.2.1 Unimodal Formulation

The problem considered in this section is a simply supported elastic column on an elastic foundation (see Fig. 1). A compressive axial force P is applied at the ends of the column, and the foundation stiffness K is assumed to be constant (Winkler-type foundation). In this optimization problem, the objective is to maximize the lowest buckling load while the total volume of the column remains fixed. The lowest buckling load P is expressed in terms of the Rayleigh quotient:

$$P = \min_{Y} \frac{\int_0^L EI(Y'')^2 dX + \int_0^L KY^2 dX}{\int_0^L (Y')^2 dX} \tag{2-27}$$

where X is the axial coordinate, L is the column length, and Y(X) is the transverse deflection.

For computational simplicity, the bending stiffness of the column, EI(X), is assumed to be proportional to the cross-sectional area A(X):

$$EI(X) = cEA(X), \tag{2-28}$$

where c is a constant. This is the case for a sandwich column or a column with constant depth and varying width[24].

Introducing non-dimensional quantities x, y(x), $\alpha(x)$, p, and k by

$$\begin{aligned} &x = \frac{X}{L}, \qquad y(x) = \frac{Y(xL)}{L}, \qquad \alpha(x) = \frac{A(xL)}{A_u}, \\ &p = \frac{PL^2}{EI_u}, \qquad k = \frac{KL^4}{EI_u} \end{aligned} \tag{2-29}$$

where A_u and EI_u correspond to a uniform column with the same total volume, the non-dimensional buckling load p is expressed as

$$p = \min_{y} \frac{\int_0^1 \alpha(y'')^2 dx + k\int_0^1 y^2 dx}{\int_0^1 (y')^2 dx} \tag{2-30}$$

and the constraint of given total volume becomes

$$\int_0^1 \alpha dx = 1. \tag{2-31}$$

Then the augmented functional p* is

$$p^* = \int_0^1 \alpha(y'')^2 dx + k\int_0^1 y^2 dx - \eta\{\int_0^1 (y')^2 dx - 1\} - \mu\{\int_0^1 \alpha dx - 1\} \tag{2-32}$$

where η and μ are Lagrange multipliers.

The buckling mode is approximated as a series of sine functions that are the buckling modes for a column with a uniform cross-section:

$$y = \sum_{i=1}^{N} b_i \sin(i\pi x) \tag{2-33}$$

where N is the number of modes.

The cross-sectional area, α, is assumed to be symmetric about the mid-span. To represent α, M equidistant nodes are selected in the region $0 < x < \frac{1}{2}$ (the first node is at $x = 1/(2M)$ and the M^{th} node is at $x = M/(2M+1)$), and α is assumed to vary linearly between the nodes. Then α is expressed as a linear combination of the a_i , where a_i denotes the cross-sectional area at node i. Also, a_i is replaced by β_i^2 to prevent the cross-sectional area, α, from having negative values. Then the augmented functional, p*, is transformed to a function which is expressed in terms of the variables β_i, b_i, μ, and η. By taking the partial derivatives of p* with respect to these variables, the first derivative conditions (equations (2-5)-(2-10)) and the second derivative conditions (equations (2-12) and (2-13)) are obtained.

2.2.2 Bimodal Formulation

The two lowest buckling loads, p_1 and p_2 , expressed by the Rayleigh quotient are

$$p_i = \frac{\int_0^1 \alpha(y_i'')^2 dx + k\int_0^1 y_i^2 dx}{\int_0^1 (y_i')^2 dx} \qquad \text{for } i = 1,\ 2 \tag{2-34}$$

where y_i are the corresponding buckling modes. The bimodality condition is treated as an equality constraint:

$$p_1 - p_2 = 0 \tag{2-35}$$

Normalizing the buckling modes y_i such that the denominators of the Rayleigh quotient are unity, the augmented functional p^* is constructed:

$$p^* = p_1 - \gamma(p_1 - p_2) - \sum_{i=1}^{2}\eta_i\{\int_0^1 (y_i')^2 dx - 1\} - \mu\{\int_0^1 \alpha dx - 1\} \tag{2-36}$$

where γ, η_1, η_2, and μ are Lagrange multipliers.

Since the model treated has symmetric boundary conditions, it is expected that the buckling modes associated with the lowest buckling loads are symmetric and anti-symmetric. Therefore the modes y_1 and y_2 are discretized as follows:

$$
\begin{aligned}
y_1 &= \sum_{i=1}^{N/2} b_i \sin(2i-1)\pi x \\
y_2 &= \sum_{i=1}^{N/2} c_i \sin(2i\pi x)
\end{aligned}
\qquad (2-37)
$$

Then the first derivative conditions and the second derivative conditions are obtained from equations (2-17)-(2-26).

2.2.3 Results and Discussion

To show how the second-order conditions work for the min-max problem, a simple example with two cross-sectional variables and two buckling mode variables is solved first. Lines #1, #2, #3, #4, and #5 in Figure 2 are non-dimensional buckling loads for solutions which satisfy the first-order conditions. The second-order conditions are checked for three foundation stiffnesses: $k = 0$, 350, and 800.

The results of the second-order conditions demonstrate their physical interpretations. For example, there are four solutions for $k = 0$, two each for two types of cross-section. The solution on line #1 gives the minimum value of the first buckling load; the one on line #2 gives the maximum value of the first buckling load; the one on line #3 gives the minimum value of the second buckling load; and the one on line #4 gives the maximum value of the second buckling load. The second-order conditions obtained are in accord with these physical interpretations: equation (2-12) is violated on lines #1 and #3, indicating that the structure can be changed to increase the buckling load, and equation (2-13) is violated on lines #3 and #4, indicating that there is a lower buckling mode. Only one solution, the one on line #2, satisfies the second variation conditions when $k = 0$, and is the true optimum. In general, whenever a solution violates equation (2-12), there exists another material distribution for which the lowest buckling load is higher, and when a solution violates equation (2-13) the buckling load is not the lowest one for the given material distribution.

A computer program was written to implement the method described in the previous sections. The program starts with $M = 2$ and $N = 5$ and increases them gradually up to $M = 16$ and $N = 40$. Table 1 shows the dependence of the solution on the number of terms in the discretization when $k = 1000$. As can be seen in Table 1, the unimodal solution has a higher buckling load than that of the bimodal solution. This is due to the discretization process which replaces the bimodal solution with two almost equal buckling loads. However, as shown in Table 1, the ratio of the first buckling load and the second buckling load for the unimodal formulation approaches unity and the buckling load converges to that of the bimodal formulation as the number of variables is increased. Also, the solution of the unimodal formulation failed for the case $M = 16$ and $N = 40$. This may indicate that a solution does not exist or that convergence is prevented by the non-linear equation solver shuttling back and forth between the two solutions.

The mode shapes and material distributions are plotted in Figure 3 for the unimodal formulation with $M = 8$, $N = 20$, $k = 0$, 500, and 1000, and in Figure 4 for the bimodal formulation with $M = 16$, $N = 40$, $k = 500$ and 1000. The results are compared with those obtained by Plaut, Johnson, and Olhoff [24] in Table 2, and show good agreement.

2.3 Optimal Foundation for Uniform Column Example

2.3.1 Unimodal Formulation

In the previous section we optimized columns which are attached to given foundations. We now consider the problem of determining the optimal foundation for a given uniform column. In this problem, the objective is to maximize the lowest buckling load while the total foundation stiffness remains fixed. The lowest buckling load P is given by equation (2-27). Introducing non-dimensional quantities k(x), p, and k_T, besides x and y(x) in equation (2-29),

$$p = \frac{PL^2}{EI}, \qquad k_T = \frac{K_T L^3}{EI}, \qquad k(x) = \frac{K(xL)L^4}{EI} \tag{2-38}$$

where K_T is the total foundation stiffness, the non-dimensional buckling load p is expressed as

$$p = \min_{y} \frac{\int_0^1 (y'')^2 dx + \int_0^1 k\, y^2 dx}{\int_0^1 (y')^2 dx} \tag{2-39}$$

and the constraint of given total foundation stiffness becomes

$$\int_0^1 k\, dx = k_T. \tag{2-40}$$

Additionally we impose the maximum foundation constraint

$$k - k_{max} \leq 0. \tag{2-41}$$

Then the augmented functional p* is

$$p^* = \int_0^1 (y'')^2 dx + \int_0^1 ky^2 dx - \eta\{\int_0^1 (y')^2 dx - 1\} - \mu\{\int_0^1 kdx - k_T\} - \int_0^1 \Lambda(x)\{k + T^2(x) - k_{max}\}dx \tag{2-42}$$

where η, μ, and $\Lambda(x)$ are Lagrange multipliers and T(x) is a slack variable.

The buckling mode is approximated as a series of sine functions (equation (2-33)). The foundation distribution, k, Lagrange multiplier, Λ, and slack variable function, T, are all assumed to be symmetric about mid-span. To represent these functions, M equidistant nodes are selected in the region $0 < x < \frac{1}{2}$ and k, Λ, and T are assumed to be constant between the nodes. The foundation stiffness in the i-th segment is denoted β_i^2 to prevent negative values. Then the augmented functional, p^*, is expressed in terms of the variables β_i, b_i, Λ_i, T_i, μ, and η. By taking the partial derivatives of p^* with respect to these variables, the first-order conditions (equations (2-5)-(2-10)) and the second-order conditions (equations (2-12) and (2-13)) are obtained.

2.3.2 Bimodal Formulation

The two lowest buckling loads, p_1 and p_2, expressed by the Rayleigh quotient are

$$p_i = \frac{\int_0^1 (y_i'')^2 dx + \int_0^1 k y_i^2 dx}{\int_0^1 (y_i')^2 dx} \qquad \text{for } i = 1,\ 2 \qquad (2-43)$$

where y_i are the corresponding buckling modes.

With the bimodality constraint (equation (2-35)), the augmented functional p^* is constructed:

$$p^* = p_1 - \gamma(p_1 - p_2) - \sum_{i=1}^{2} \eta_i \{ \int_0^1 (y_i')^2 dx - 1 \} - \mu \{ \int_0^1 k dx - k_T \} - \int_0^1 \Lambda(x) \{ k + T^2(x) - k_{max} \} dx \qquad (2-44)$$

where γ, η_1, η_2, μ and $\Lambda(x)$ are Lagrange multipliers.

The buckling modes y_1 and y_2 are discretized using equations (2-37). Then the first-order conditions and the second-order conditions are obtained from equations (2-17)-(2-26).

2.3.3 Results and Discussion

The program starts with $M = 2$ and $N = 6$ and increases them gradually up to $M = 16$ and $N = 48$. Figure 5 shows foundation distributions for various values of M and N at $k_T = 1{,}000$ and $k_{max} = 2{,}000$. Again it is observed that the bimodal solutions are lower. The total CPU time (IBM 3084) when $k_t = 400$ for $M = 16$ and $N = 48$ was 39.7 seconds with the unimodal formulation and 36.7 seconds with the bimodal formulation.

For $M = 16$, $N = 48$, and several combinations of k_T and k_{max}, the optimal foundation distributions and corresponding mode shapes are plotted in Figure 6 for the unimodal formulation and in Figure 7 for the bimodal formulation. In Figure 6, the optimal solution tends to place foundation stiffness in regions where the buckling mode has its largest deflections. In Figure 7, the mode shape with the highest number of maxima and minima seems to govern the placement of the foundation stiffness. For instance, if $k_T = 1000$ and $k_{max} = 2000$, there is no stiffness in the central region where the symmetric mode has its largest deflection, and the stiffness is located about the locations of the maximum and minimum of the anti-symmetric mode.

For a uniform pinned-pinned column attached to a uniform foundation, the buckling load is as follows[28]: for the integer n such that

$$(n-1)^2 n^2 \pi^4 \le k_T \le n^2 (n+1)^2 \pi^4, \qquad (2-45)$$

we have

$$p_{unif} = n^2 \pi^2 + \frac{k}{n^2 \pi^2}. \qquad (2-46)$$

The buckling loads associated with the optimal foundations are compared with those for uniform foundations in Table 3. The increase in buckling load due to an optimization of the foundation stiffness distribution can be substantial.

Table 1. Nondimensional buckling loads for different numbers of variables (k = 1000)

M x N	2 x 5	4 x 10	8 x 20	16 x 40
Buckling loads (bimodal)		70.400	73.040	73.008
Buckling loads (unimodal)	74.999	72.719	73.051	
Ratio of the first two buckling loads(unimodal)	0.7352	0.8182	0.9660	

Table 2. Nondimensional buckling loads of optimum columns with different foundation stiffnesses

k	0	500	1000
Plaut et al.[24]	12.0	58.6	71.9
Current study	12.0	59.3	73.0

Table 3. Nondimensional buckling loads for optimum and uniform foundations ($M = 16$, $N = 48$)

k_T	k_{max}	Buckling load p (unimodal results)	p_{unif}	% increase
100	2000	29.3	20.0	47
400	2000	57.6	49.6	16
1000	2000	80.8	64.9	25
4000	20000	154.4	133.9	15

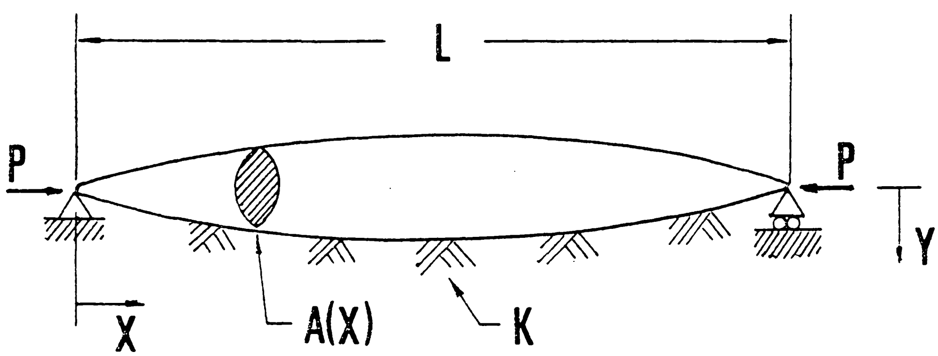

Figure 1. Geometry of Column and Foundation

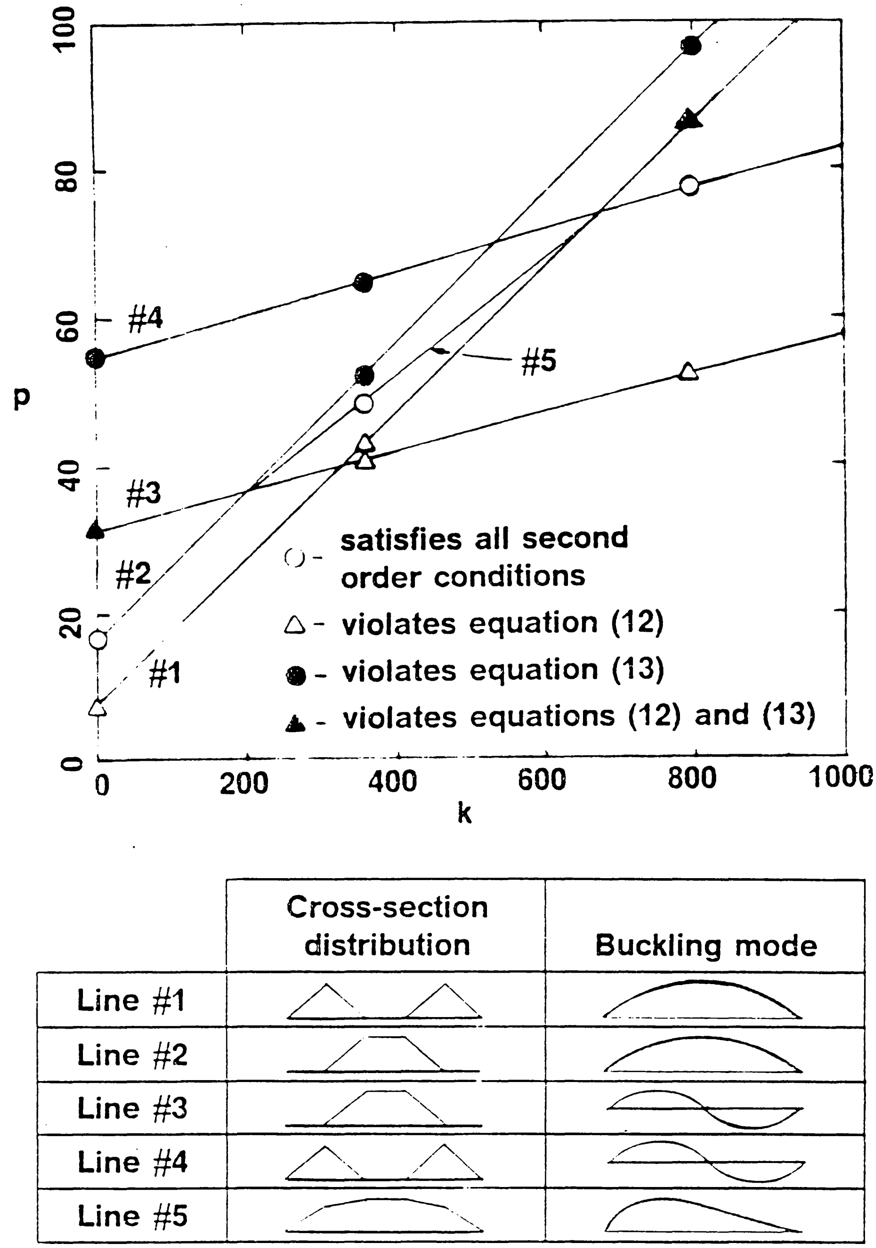

Figure 2. Example Using M = 2, N = 2

k	p	Cross-section distribution	Buckling mode
0	12.0		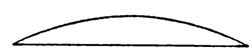
500	59.4	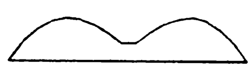	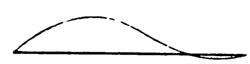
1000	73.1		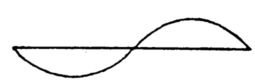

Figure 3. Unimodal Optimum Designs for Beam-Column with Fixed Foundation (M = 8, N = 20)

k	p	Cross-section distribution	Buckling mode
500	59.3		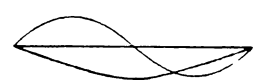
1000	73.0	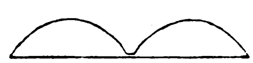	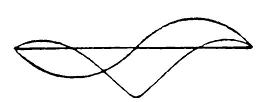

Figure 4. Bimodal Optimum Designs for Beam-Column with Fixed Foundation ($M = 16$, $N = 40$)

	Unimodal results		Bimodal results	
M x N	p	Foundation distribution	p	Foundation distribution
2 x 6	64.8	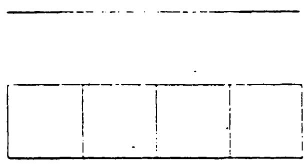	64.3	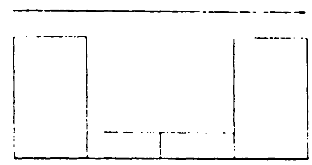
4 x 12	80.8	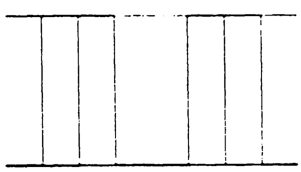	77.6	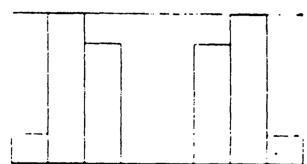
8 x 24	80.8	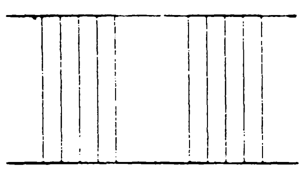	80.0	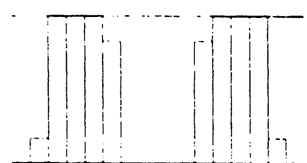
16 x 48	80.8	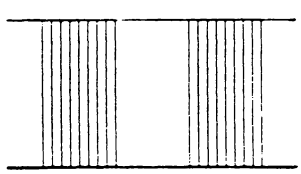	80.5	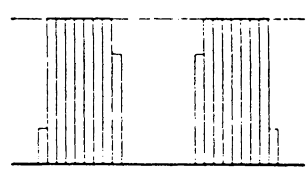

Figure 5. Optimum Foundation Designs for Unimodal and Bimodal Foundations (k_T = 1000, k_{max} = 2000)

k_T ($k_{max.}$)	p	Foundation distribution	Buckling mode
100 (2000)	29.3	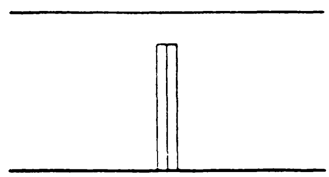	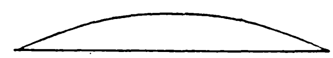
400 (2000)	57.6	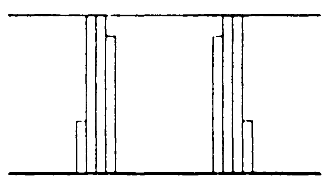	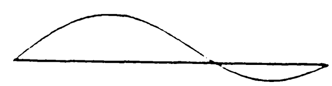
1000 (2000)	80.8	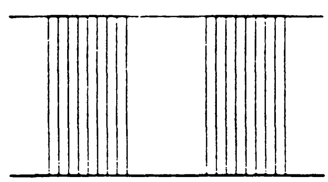	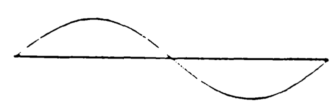
4000 (20000)	154.4	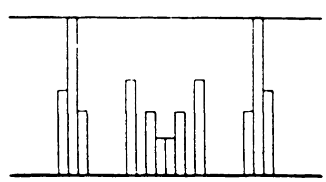	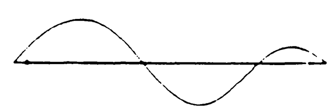

Figure 6. Optimum Foundation Designs for Unimodal Formulation ($M = 16$, $N = 48$)

k_T ($k_{max.}$)	p	Foundation distribution	Buckling modes
400 (2000)	57.6	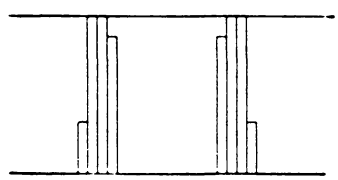	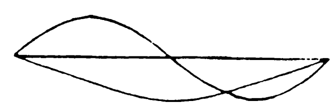
1000 (2000)	80.5	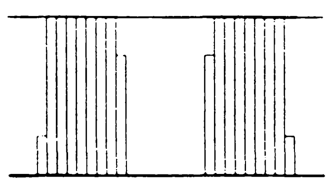	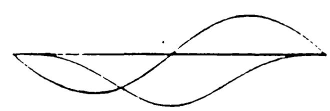
4000 (20000)	154.4	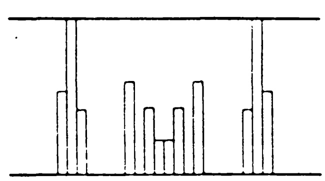	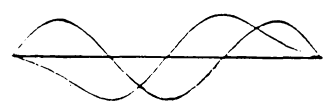

Figure 7. Optimum Foundation Designs for Bimodal Formulation (M = 16, N = 48)

Chapter 3

Tracing Optima

Optimization problems are typically solved by starting with an initial estimate and proceeding iteratively to improve it until the optimum is found. The design points along the path from the initial estimate to the optimum are usually of no value. However, this need not be the case. In many applications, it is of interest to find the family of optima obtained by varying an input parameter such as the amount of available resources. If one member of the family is known, it may be possible to use it as a starting point and to follow an optimization path that goes through the other members of the family.

The optimization procedure proposed in the previous chapter addressed the problem of identifying the optimal solution by first identifying it for a crude mesh and then gradually refining the mesh. This did not always work well. The present chapter pursues this idea further by proposing that we first find the optimum for a simple case and then gradually change the simple case to the one we want. If the parameter used for the change is of physical interest we get a bonus of a complete path of optima.

A first step in tracing a family of optima is the application of sensitivity information to extrapolate from one member of the family to another. The present chapter proposes the use of the sensitivity information to formulate the path of optima as the trajectory of a differential equation, a procedure known as a homotopy technique.

In this chapter, the original globally convergent homotopy method is adapted to the design of an elastic foundation for maximizing the buckling load of a column. This problem was solved in Chapter 2 for a limited range of resource (i.e., total foundation stiffness). This study shows how the solution process can start from the minimum amount of resources which is required for a feasible solution to the highest value that may be of interest.

3.1 Formulation

3.1.1 Optimization Problem

The optimization problem that we consider here is to maximize the lowest buckling load of a structure for a given amount of resources. The structure is discretized by finite elements. Expressing the lowest buckling load with Rayleigh's quotient, the problem is written as

$$\max_{v} \quad \min_{u} \quad \frac{u^T K u}{u^T K_G u} \qquad (3-1)$$

such that $c^T v - \theta = 0$

and $v_{i\,min} \leq v_i \leq v_{i\,max}$ for $i = 1, \ldots, M$

where v is a vector of design variables with components v_i, u is the displacement vector, K and K_G are the stiffness matrix and the geometric stiffness matrix, respectively, c is a positive cost vector, and θ is the amount of available resources, representing total foundation stiffness. The M design variables are subject to upper and lower bounds, $v_{i\,max}$ and $v_{i\,min}$, respectively.

A typical optimization method, applied to solve this problem, starts from a given design and continuously searches for better designs until it finds an optimum design. The trial designs along the path are of no value. The proposed method instead proceeds along a path of optimal designs for increasing amounts of resource θ. The resource θ is varied between the minimum θ_{min} required to satisfy the lower bound constraints and a maximum θ_{max} when all variables are at their upper bounds.

The path consists of several smooth segments, each segment being characterized by a set I_A of variables which are at their upper or lower bounds. Along each segment, some inequality constraints can be treated as equality constraints,

$$v_j = v_{j\,min} \quad \text{or} \quad v_j = v_{j\,max} \qquad \text{for } j \in I_A \tag{3-2}$$

so that these variables can be eliminated from the optimization problem, while the other variables do not have to be constrained. The optimization problem along a segment can, therefore, be written as

$$\max_{v_i} \quad \min_{u} \quad \frac{u^T K u}{u^T K_G u} \qquad \text{for } i \notin I_A \tag{3-3}$$

such that $c^T v - \theta = 0$.

The solution of the problem consists of three related problems: solving the optimization problem along a segment, locating the end of the segment where the set I_A changes, and finding the set I_A for the next segment.

3.1.2 Stationary conditions

It is common practice to normalize the displacement vector u such that the denominator of Rayleigh's quotient is unity and to treat this as an equality constraint. Then, using Lagrange multipliers η and μ, the augmented function P* is formed:

$$P* = u^T K u - \eta[u^T K_G u - 1] - \mu[c^T v - \theta] \qquad (3-4)$$

The following stationary conditions are obtained by taking the first derivative of P* with respect to v_i, u, η, and μ, and setting it equal to zero:

i) Optimality conditions

$$u^T \frac{\partial K}{\partial v_i} u - \eta u^T \frac{\partial K_G}{\partial v_i} u - \mu c_i = 0 \qquad \text{for } i \notin I_A \qquad (3-5)$$

ii) Stability conditions

$$Ku - \eta K_G u = 0 \qquad (3-6)$$

iii) Normalization constraint

$$1 - u^T K_G u = 0 \qquad (3-7)$$

iv) Total resource constraint

$$\theta - c^T v = 0 \qquad (3-8)$$

Equations (3-5)-(3-8) form a system of nonlinear equations to be solved for v_i , u, η, and μ. A homotopy method is used to find the solutions of these equations as a function of θ.

In certain ranges of structural resources, the optimal solution is known to be bimodal, i.e., the lowest buckling load is a repeated eigenvalue. The existence of bimodal solutions also introduces additional transitions (bimodal to unimodal and vice versa) along the path of optimum solutions. The formulation for bimodal solutions follows.

To seek the solutions with double eigenvectors, the problem is to be formulated assuming bimodality of solutions, or equality of the two lowest eigenvalues, P_1 and P_2. They are expressed in terms of the Rayleigh quotient:

$$P_i = \frac{u_i^T K\, u_i}{u_i^T K_G u_i} \qquad \text{for } \; i = 1, \; 2$$

where u_i are the corresponding eigenvectors.

Treating the bimodality condition as an equality constraint, $P_1 - P_2 = 0$, the augmented function $P*$ is formed:

$$P* = u_1^T K\, u_1 - \gamma[u_1^T K\, u_1 - u_2^T K\, u_2] - \sum_{i=1}^{2} \eta_i [u_i^T K_G\, u_i \; - \; 1] - \mu[c^T v - \theta].$$

The stationary conditions are obtained by taking the first derivatives of $P*$ with respect to v_i, u, γ, η_1, η_2, and μ and setting them to zero. Thus we obtain

i) Optimality conditions

$$(1-\gamma)u_1^T \frac{\partial K}{\partial v_i} u_1 + \gamma u_2^T \frac{\partial K}{\partial v_i} u_2 - \eta_1 u_1^T \frac{\partial K_G}{\partial v_i} u_1 - \eta_2 u_2^T \frac{\partial K_G}{\partial v_i} u_2 - \mu c_i = 0 \qquad \text{for } \; i \notin I_A$$

ii) Stability conditions

$$(1-\gamma)Ku_1 - \eta_1 K_G u_1 = 0$$
$$\gamma K u_2 - \eta_2 K_G u_2 = 0$$

iii) Bimodality constraint

$$u_2^T K u_2 - u_1^T K u_1 = 0$$

iv) Normalization constraints

$$1 - u_1^T K_G u_1 = 0$$
$$1 - u_2^T K_G u_2 = 0$$

v) Total resource constraint

$$\theta - c^T v = 0.$$

3.2 Homotopy method

The system of equations with a homotopy parameter θ has the form

$$F(x, \theta, d) = 0 \qquad (3-9)$$

where θ is a positive real number, F, x, and d are N-dimensional vectors and N is the number of degrees of freedom. Note that F is viewed as a function of x(the design vector), θ (the resource parameter), and d(the parameter vector, usually a random imperfection; see, e.g., reference [17]). The theoretical basis for globally convergent homotopy algorithms is the following fact from differential geometry [9].

Theorem: Suppose that the N x (2N + 1) Jacobian matrix of F has full rank on

$$F^{-1}(0) = \{(x, \theta, d) \mid F(x, \theta, d) = 0, \theta_a < \theta < \theta_b\}.$$

Then for almost all N-vectors d (i.e., except those in a set of Lebesgue measure zero), the N x (N + 1) Jacobian matrix of

$$\tilde{F}(x, \theta) = F(x, \theta, d)$$

also has full rank on

$$\tilde{F}^{-1}(0) = \{(x, \theta) \mid \tilde{F}(x, \theta) = 0, \theta_a < \theta < \theta_b\}.$$

Alternatively, if d were picked at random, it is virtually always true that the Jacobian matrix has full rank on the solution set of

$$\tilde{F}(x, \theta) = 0. \tag{3-10}$$

According to the theory in [9], this full rank of the Jacobian matrix implies that the zero set of equations (3-10) contains a smooth curve Γ in (N + 1)-dimensional (x, θ) space, which has no bifurcations and is disjoint from other zeros of (3-10). The curve Γ can be parameterized by the arc length s as

$$\begin{aligned} x &= x(s) \\ \theta &= \theta(s). \end{aligned} \tag{3-11}$$

Taking the derivative of equations (3-10) with respect to arc length, the nonlinear system of equations is transformed to a set of ordinary differential equations,

$$\left[\tilde{F}_x(x(s), \theta(s)) \;\; \tilde{F}_\theta(x(s), \theta(s))\right] \begin{bmatrix} \dfrac{dx}{ds} \\ \dfrac{d\theta}{ds} \end{bmatrix} = 0, \tag{3-12}$$

and

$$\left\| \begin{bmatrix} \frac{dx}{ds} \\ \frac{d\theta}{ds} \end{bmatrix} \right\| = 1, \qquad (3-13)$$

where $\tilde{F}_x$ and $\tilde{F}_\theta$ denote the partial derivatives of $\tilde{F}$ with respect to x and θ, respectively. With the initial conditions at $s = 0$,

$$\begin{aligned} x(0) &= x_o \\ \theta(0) &= \theta_a, \end{aligned} \qquad (3-14)$$

equations (3-12)-(3-14) can be treated as an initial value problem. We have thus converted the system of equations (3-9), parameterized by the vector d, to the initial value problem (3-12)-(3-14) whose trajectory gives the path of optimal solutions x. This technique differs significantly from standard continuation, imbedding or incremental methods in that the resource parameter, θ, is a dependent variable which can both increase and decrease along the path Γ. Also, no attempt is made to invert the Jacobian matrix $\tilde{F}_x$ so that limit points pose no special difficulty. It differs from initial value or parameter differentiation methods also, since arc length s, rather than θ, is the controlling parameter. The homotopy method is similar in spirit to the Riks/Wempner[29, 30] and Crisfield[31] methods, but the supporting mathematical theory and implementation details are very different, and the emphasis is on ordinary differential equation techniques rather than a Newton-type iteration.

The homotopy method as described in references [9-18] is intended to solve a <u>single</u> nonlinear system of equations, and converge from an arbitrary starting point with probability one. In this context $\theta \in [0, 1]$, and the zero curve Γ is bounded and leads to the (single) desired solution at $\theta = 1$. The d vector, viewed as an artificial perturbation of the problem, plays a crucial role. In the version of the method employed here, $\theta \in (\theta_a, \theta_b)$, <u>each</u> point along Γ has physical significance, and d is fixed at zero (no perturbation). Because d is not random, the claimed properties for Γ hold only in subintervals (θ_a, θ_b) of $[0, \infty)$. Detecting and dealing with these subinterval transition points is the essence of the modification of the homotopy method used in the present paper.

There are several approaches to tracking the curve Γ, which along with theoretical background can be found in Watson[32]. A software package, HOMPACK, which implements several different homotopy algorithms is under development at Sandia National Laboratories, General Motors Research Laboratories, Virginia Polytechnic Institute and State University, and the University of Michigan. One of the HOMPACK subroutines, FIXPNF, is used in the current work.

3.3 Switching from one Segment to the Next

There are four types of events which end a segment and start a new one:

Type 1: A bound constraint becoming active (i.e., being satisfied as an equality),

Type 2: A bound constraint becoming inactive,

Type 3: Transition from a unimodal solution to a bimodal solution,

Type 4: Transition from a bimodal solution to a unimodal solution.

To switch from one segment to the next, we first need to locate the transition point. At a transition point there are a number of solution paths which satisfy the stationary equations, and we need to choose the optimum path.

3.3.1 Locating the transition points

Transition points are located by checking the bound constraints and the optimality conditions.

The bound constraints

$$v_{i\,min} \le v_i \le v_{i\,max} \qquad \text{for } i = 1, \ldots, M \tag{3-15}$$

are checked to detect a transition point of type 1.

Optimality of the solution is checked by the Kuhn-Tucker conditions and the second-order conditions discussed below. The solution satisfies the Kuhn-Tucker conditions when all Lagrange multipliers are nonnegative. So a transition of type 2 is detected by checking the positivity of the Lagrange multipliers associated with the bound constraints. These multipliers are obtained by adding the bound constraints to the formulation (3-3) and replacing the augmented function P* by

$$P* = u^T K u - \eta[u^T K_G u - 1] - \mu[c^T v - \theta] - \sum_{i \in I_A} \lambda_{1i}[v_{i\,min} - v_i] - \sum_{i \in I_A} \lambda_{2i}[v_i - v_{i\,max}]. \tag{3-16}$$

Taking the first derivative of P* with respect to v_i gives

$$u^T \frac{\partial K}{\partial v_i} u - \eta u^T \frac{\partial K_G}{\partial v_i} u - \mu c_i + \lambda_{1i} - \lambda_{2i} = 0 \qquad \text{for } i \in I_A. \tag{3-17}$$

Since λ_{1i} is 0 for $v \neq v_{i\,min}$ and λ_{2i} is 0 for $v_i \neq v_{i\,max}$ for the above equations, λ_{1i} and λ_{2i} are given by

$$\begin{aligned} \lambda_{1i} &= -u^T \frac{\partial K}{\partial v_i} u + \eta u^T \frac{\partial K_G}{\partial v_i} u + \mu c_i && \text{for } v_i = v_{i\,min} \\ \lambda_{2i} &= u^T \frac{\partial K}{\partial v_i} u - \eta u^T \frac{\partial K_G}{\partial v_i} u - \mu c_i && \text{for } v_i = v_{i\,max}. \end{aligned} \tag{3-18}$$

A type 2 transition is detected by a Lagrange multiplier becoming nonpositive. Similar equations for the bimodal case are obtained by adding the bound constraints to the augmented function P* and taking the first derivatives of P* with respect to v_i . They are given by

$$\lambda_{1i} = -(1-\gamma)u_1^T \frac{\partial K}{\partial v_i} u_1 - \gamma u_2^T \frac{\partial K}{\partial v_i} u_2 + \eta_1 u_1^T \frac{\partial K_G}{\partial v_i} u_1 + \eta_2 u_2^T \frac{\partial K_G}{\partial v_i} u_2 + \mu c_i \qquad \text{for } v_i = v_{i\,min}$$

$$\lambda_{2i} = (1-\gamma)u_1^T \frac{\partial K}{\partial v_i} u_1 + \gamma u_2^T \frac{\partial K}{\partial v_i} u_2 - \eta_1 u_1^T \frac{\partial K_G}{\partial v_i} u_1 - \eta_2 u_2^T \frac{\partial K_G}{\partial v_i} u_2 - \mu c_i \qquad \text{for } v_i = v_{i\,max}.$$

The bimodal formulation replaces η by η_1 and η_2 which are the Lagrange multipliers for the normalization constraints on the two buckling modes. When one of them becomes negative, the corresponding mode should be removed for the optimum design, so that we have a transition of type 4 from bimodal to unimodal design.

For a transition of type 3, we need to check if there is another buckling mode associated with a lower buckling load. This can be accomplished by checking the second-order optimality conditions for the buckling mode variables u given by

$$\begin{aligned} &r^T\,[\nabla_u^2 P*]\,r > 0 \qquad \text{for every } r \text{ such that} \\ &\qquad \nabla_u h^T\, r = 0 \end{aligned} \qquad (3-19)$$

$$\text{where} \quad [\nabla_u^2 P*] = \left[\frac{\partial^2 P*}{\partial u_s\, \partial u_t} \right]$$

$$\nabla_u h = \left\{ \frac{\partial h}{\partial u_s} \right\}$$

$$h = u^T K_G\, u - 1.$$

Alternatively we can solve the buckling problem (3-6) for the current design and check whether the buckling load obtained from the stationary conditions is truly the lowest one. The transition of type 3 is detected by checking if

$$p \neq p_1 \qquad (3-20)$$

where p is the buckling load obtained from the stationary conditions while p_1 is the first buckling load obtained by solving the stability conditions (3-6) for the given structure.

3.3.2 Choosing an optimum path

Once a transition point is located, we need to choose a path which satisfies the optimality conditions. Choosing an optimum path constitutes finding a set of active bound constraints for type 1 and 2 transitions and the correct buckling modes for type 3 and 4 transitions. These are obtained by using the Lagrange multipliers of the previous path and the sensitivity calculation on the buckling load. The procedure is explained separately for each type of transition.

A type 1 transition occurs when one of design variables, v_i, hits the upper or lower bound. Then v_i is set at $v_{i\,max}$ or $v_{i\,min}$ and treated as a constant value. The number of design variables is reduced by one.

At a type 2 transition, one of the Lagrange multipliers for the bound constraints, λ_{1i} and λ_{2i}, is found to be negative. The bound constraint corresponding to the negative λ_{1i} or λ_{2i} is set to be inactive and the number of design variables is increased by one.

At a transition from a unimodal solution to a bimodal solution (a type 3 transition), the formulation requires two buckling modes, u_1 and u_2, for the solution of the upcoming bimodal path. These modes can be obtained by solving the stability conditions (3-6) of the previous unimodal formulation, since the stability conditions give two buckling modes at the bimodal transition point.

At a transition from a bimodal to a unimodal solution (a type 4 transition), two buckling modes are given from the bimodal solution. One of the Lagrange multipliers for the normalization constraints, η, is known to be negative from the previous transition check, so the buckling mode corresponding to the positive η is chosen.

Some of the above transitions can occur simultaneously. Special treatment is required in certain cases where the Lagrange multipliers are not available. In general, the optimum design requires at least one design variable v_i for a unimodal case and two design variables for a bimodal case. At a type 1 transition, the number of design variables is reduced by one, and at a type 3 transition the bimodal formulation requires one more design variable in case the previous unimodal path has only one design variable. So some type 1 or type 3 transitions occur simultaneously with a type 2 transition which allows an additional design variable. In that case, the Lagrange multipliers λ_{1i} and λ_{2i}, which are used at a type 2 transition to determine a new design variable, are not available. We then rely on the sensitivity information of p with respect to v. For a unimodal case, the location of the new design variable v_i is determined where $\frac{dp}{d\theta}$ is maximized. For a bimodal case, we need to find a combination of i and j which maximizes the value of the bimodal buckling load for a small increment of the total available resource. Considering the bound constraints in the formulation, the new design variables are determined by

$$\max_{i,\,j} \quad \frac{dp}{d\theta} = \frac{\partial p_1}{\partial v_i}\frac{dv_i}{d\theta} + \frac{\partial p_1}{\partial v_j}\frac{dv_j}{d\theta} \tag{3-21}$$

$$\begin{aligned}
\text{such that} \quad & \frac{\partial p_1}{\partial v_i}\frac{dv_i}{d\theta} + \frac{\partial p_1}{\partial v_j}\frac{dv_j}{d\theta} = \frac{\partial p_2}{\partial v_i}\frac{dv_i}{d\theta} + \frac{\partial p_2}{\partial v_j}\frac{dv_j}{d\theta} \\
& \frac{dv_i}{d\theta} \geq 0 \quad \text{for } v_i = v_{i\,min} \\
& \frac{dv_i}{d\theta} \leq 0 \quad \text{for } v_i = v_{i\,max} \\
& \frac{dv_j}{d\theta} \geq 0 \quad \text{for } v_j = v_{j\,min} \\
\text{and} \quad & \frac{dv_j}{d\theta} \leq 0 \quad \text{for } v_j = v_{j\,max}
\end{aligned}$$

where p_1 and p_2 are the buckling loads corresponding to the buckling modes u_1 and u_2, respectively.

After we obtain the design variables v and the buckling modes u, we need the Lagrange multipliers μ, η, and γ at the transition point to complete the set of starting values for the next solution path. These are obtained by solving the stationary conditions for the given u and v. For example, in the unimodal case, η is obtained from the stability conditions (3-6) and μ is obtained by solving one of the optimality conditions (3-5).

3.4. Optimal Foundation for Uniform Column Example

The example used to demonstrate the tracing procedure is a simply supported column on an elastic foundation taken from the previous chapter.

The design problem is to find the optimum distribution of the foundation to maximize the lowest buckling load. The design variable is the foundation stiffness. The column is modeled by sixteen beam finite elements and the foundation stiffness for each element is assumed to be constant. The geometry of the column and the foundation is shown in Fig. 8. Because of the symmetry of the problem, the foundation distribution is assumed to be symmetric, so there are eight design variables, $K_1, \ldots, K_8$. The constraint of the total foundation stiffness is given by

$$\frac{1}{8}\sum_{i=1}^{8} K_i = K_T \tag{3-22}$$

where K_T is the total foundation stiffness used as the homotopy parameter.

The upper and lower bound constraints are given by

$$K_{min} \le K_i \le K_{max} \qquad \text{for } i = 1, \ldots, 8 \tag{3-23}$$

where K_{min} is the lower bound and K_{max} is the upper bound of the foundation stiffness. The buckling load P and the foundation stiffness parameters are expressed in nondimensional form as

$$p = \frac{PL^2}{EI}, \quad k_i = \frac{K_i L^4}{EI}, \quad k_{min} = \frac{K_{min} L^4}{EI}, \quad k_{max} = \frac{K_{max} L^4}{EI}, \quad k_T = \frac{K_T L^4}{EI} \quad (3-24)$$

where EI is the bending stiffness of the column. The lower bound k_{min} is set at 0 and the upper bound k_{max} is set at 20,000. The procedure starts with a uniform column without any foundation material (the total nondimensional foundation stiffness k_T is zero) and optimum designs are obtained for values of k_T up to 20,000.

Figure 9 shows the buckling loads corresponding to optimum designs obtained for $0 \le k_T \le 20{,}000$. This curve has 18 transition points and consists of 19 solution paths denoted by the letters A through S. The circles on the curve indicate the transition points and the dots are the solutions traced along the optimum path. The solutions on the first path A and the last path S are unimodal and the other solutions are bimodal. This is due to the fact that the starting point of $k_T = 0$ and the last point of $k_T = 20{,}000$ are uniform designs (with unimodal solutions) in which foundations are all at the lower or at the upper bound. The buckling loads for a uniform foundation are also shown in Fig. 9 (dashed line). Note that the two curves meet at the last point where all design variables are at their upper bound and the only feasible design is uniform.

One point from each path in Fig. 9 is selected, and the optimum foundation distribution and corresponding buckling mode for these points are shown in Fig. 10 - Fig. 13.

At the starting point of $k_T = 0$, the column has no foundation at all. So we need to find a column element at which the foundation is placed when we increase k_T. Since Lagrange multipliers λ_{1i} and λ_{2i} are not available at this point, it is treated the same as if a type 1 transition occurs simultaneously with a type 2 transition. For this example, a foundation is initially placed at the mid-span where $\frac{dp}{dk_T}$ is maximum.

The unimodal solution becomes bimodal at the transition point AB from path A to path B (this is a type 3 transition). This requires one more design variable because the previous unimodal path has only one design variable (a type 2 transition occurs at the same time). At transition points BC, CD, DE, and EF, one of the foundation stiffnesses becomes zero (the lower bound) and another foundation stiffness becomes nonzero. Each of these points is a simultaneous transition of types 1 and 2 in the bimodal solution, requiring the solution of equation (3-21). At transition points FG, GH, IJ, JK, MN, OP, and QR, new variables become nonzero. These are type 2 transitions where the lower bound constraint becomes inactive. At transition points HI, KL, LM, NO, and PQ, one of the foundation stiffnesses hits the lower or upper bound. These are type 1 transitions. The last transition (RS) is a type 4 transition at which the bimodal solution becomes unimodal.

Most of the computational effort of tracing the optima is associated with the evaluation of the Jacobian matrix. The curve of Fig. 9 required about 200 integration steps to trace, each requiring 1 to 3 (mostly 1) Jacobian evaluations. The Jacobian was evaluated numerically, using forward finite differences.

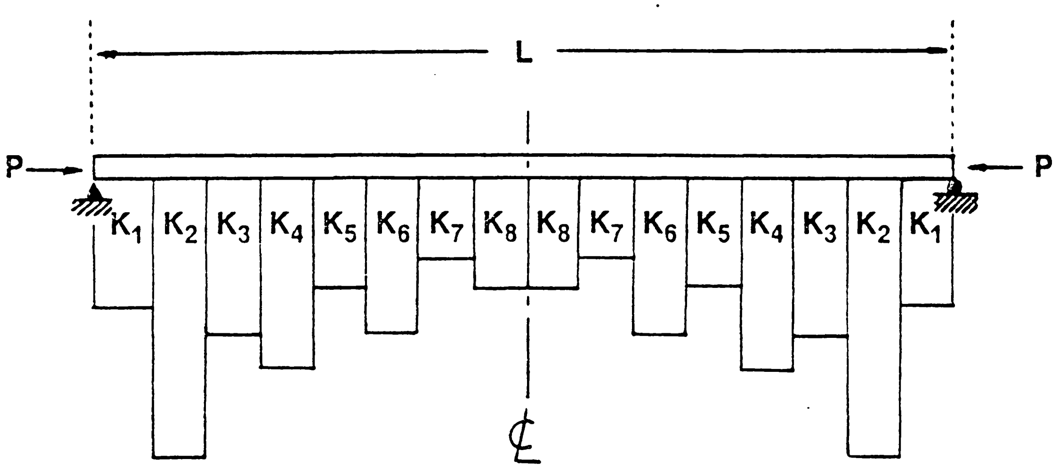

Figure 8. Geometry of Column and Foundation

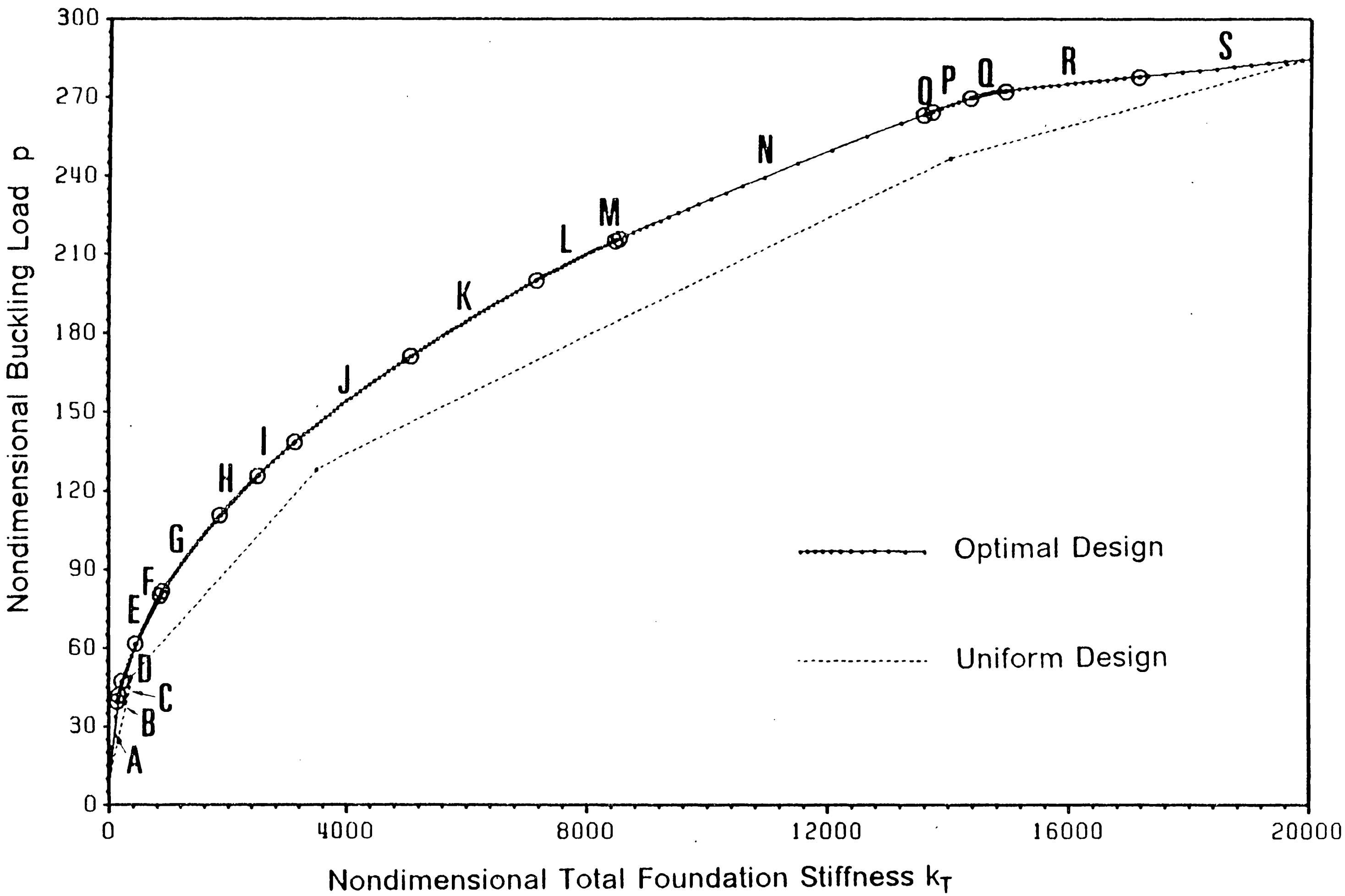

Figure 9. Nondimensional Buckling Load vs. Total Foundation Stiffness

k_T (path)	p	Foundation	Buckling mode
160.0 (A)	39.8	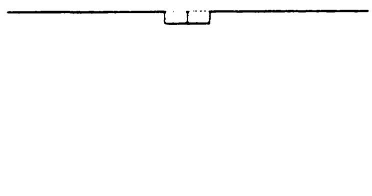	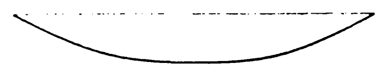
168.4 (B)	40.8	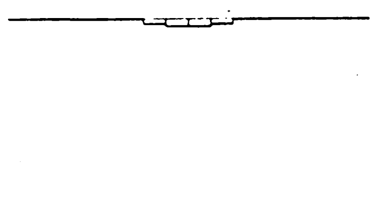	
218.1 (C)	45.6	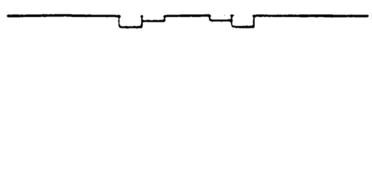	
336.4 (D)	53.9	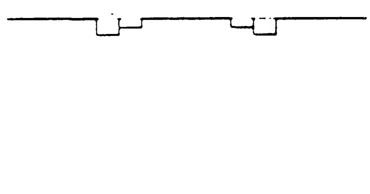	
771.0 (E)	75.9	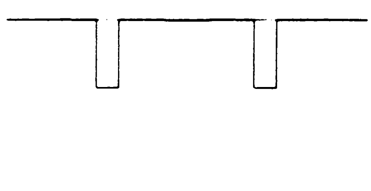	

Figure 10. Optimum Foundation Designs for Increasing Values of Total Foundation Stiffness

k_T (path)	p	Foundation	Buckling mode
927.0 (F)	82.2	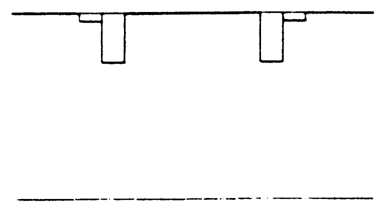	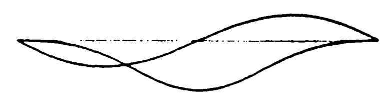
1195.1 (G)	91.2	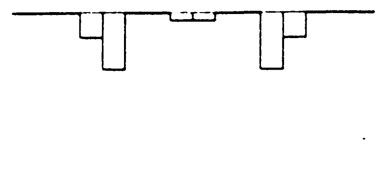	
2149.3 (H)	117.5	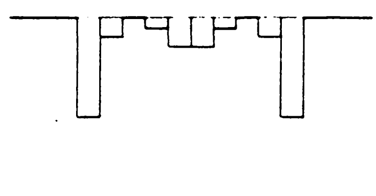	
3027.6 (I)	136.5	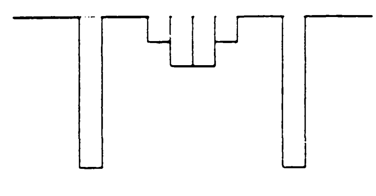	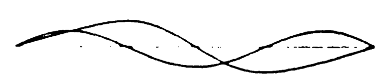
4729.4 (J)	165.7	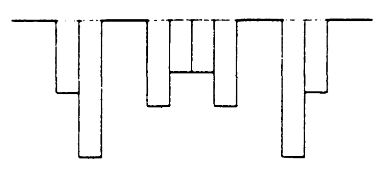	

Figure 11. Optimum Foundation Designs for Increasing Values of Total Foundation Stiffness (continued)

k_T (path)	p	Foundation	Buckling mode
6076.0 (K)	185.5	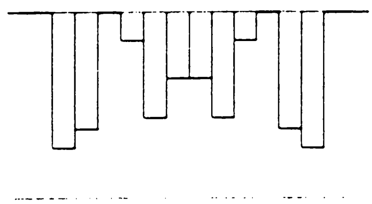	
7325.2 (L)	202.1	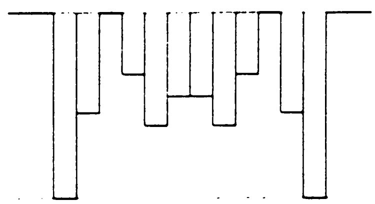	
8502.2 (M)	215.6	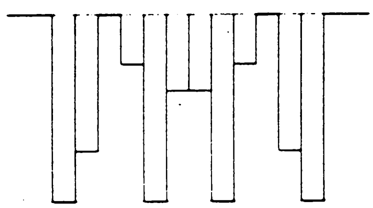	
10949.5 (N)	239.7	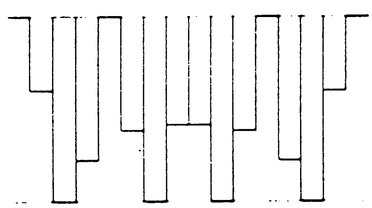	
13642.5 (O)	264.1	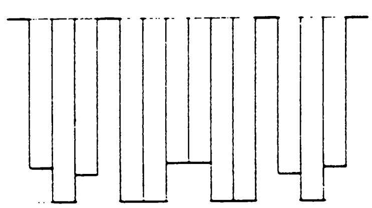	

Figure 12. Optimum Foundation Designs for Increasing Values of Total Foundation Stiffness (continued)

k_T (path)	p	Foundation	Buckling mode
14054.4 (P)	267.5	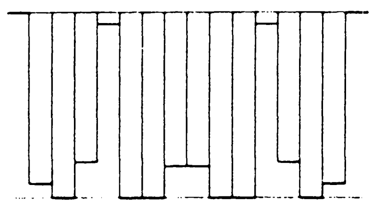	
14762.5 (Q)	272.3	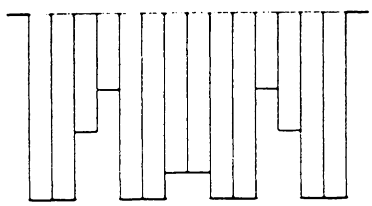	
16073.4 (R)	275.5	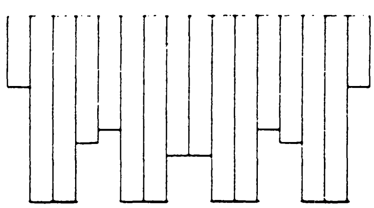	
17858.0 (S)	279.7	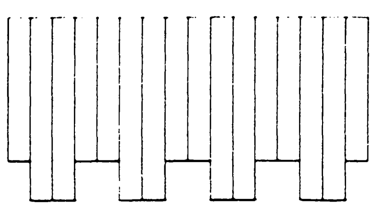	

Figure 13. Optimum Foundation Designs for Increasing Values of Total Foundation Stiffness (continued)

Chapter 4

Equivalence of Unstiffened Plate Designs with Different Stacking Sequences

Composite materials are ideal for structural applications where high strength-to-weight and stiffness-to-weight ratios are required. Design optimization of composite structures has gained importance in recent years as the engineering applications of fiber-reinforced materials have increased and weight savings has become an essential design objective, especially for aircraft and spacecraft structures.

Previous work on the optimal design of composite plates has focused on optimization with respect to the fiber orientations [33-42]. In Refs. [43-48], however, laminate optimization is considered, in which the thicknesses of plies with specified orientation angles are treated as the design variables. The thickness of material at each preassigned orientation is treated as a continuous variable. More sophisticated approaches dealing with discrete values for the thicknesses by employing integer variables are presented by Mesquita and Kamat [49, 50] and Olson and Vanderplaats [51].

The present study avoids the difficulties associated with discrete or integer variables by treating the thickness variables as continuous variables.

In this chapter, we study the effect of the stacking sequence on the optimum design and we prove a useful result on the equivalence of plates with different stacking sequences.

4.1 Equivalent Bending Stiffnesses in the Laminated Plates

4.1.1 Bending Stiffnesses from the Classical Lamination Theory

The laminates considered in this study are symmetric about the middle surface, so that the bending response is not coupled to the membrane action. The moment-curvature relations are then expressed in the form

$$\{M\} = \begin{Bmatrix} M_X \\ M_Y \\ M_{XY} \end{Bmatrix} = \begin{bmatrix} D_{11} & D_{12} & D_{16} \\ D_{12} & D_{22} & D_{26} \\ D_{16} & D_{26} & D_{66} \end{bmatrix} \begin{Bmatrix} \kappa_X \\ \kappa_Y \\ \kappa_{XY} \end{Bmatrix} = [D]\{\kappa\}, \tag{4-1}$$

where [D] is the laminate bending stiffness matrix, {M} is the bending and twisting moments per unit length, and $\{\kappa\}$ is the corresponding curvatures given by

$$\begin{Bmatrix} \kappa_X \\ \kappa_Y \\ \kappa_{XY} \end{Bmatrix} = \begin{Bmatrix} -\dfrac{\partial^2 W}{\partial X^2} & -\dfrac{\partial^2 W}{\partial Y^2} & -2\dfrac{\partial^2 W}{\partial X \partial Y} \end{Bmatrix}^T. \tag{4-2}$$

Figure 14 shows the geometry of a laminate with 2n layers. The Z axis is taken perpendicular to the midplane of the laminate and is positive in the downward direction. Below the midplane, the value of Z at the bottom of layer k is denoted Z_k. The thicknesses of the layers are given by

$$T_i = Z_i - Z_{i+1}, \qquad \text{for } i = 1, 2, \ldots, n, \tag{4-3}$$

with $Z_{n+1} = 0$.

Using classical lamination theory, the bending stiffness matrix [D] in Eq. (1) can be written as

$$[D] = \frac{2}{3} \sum_{k=1}^{n} [\overline{Q}]_k (Z_k^3 - Z_{k+1}^3), \tag{4-4}$$

where $[\overline{Q}]_k$ is the transformed reduced stiffness matrix of the k-th layer, which can be defined in terms of the ply angle ϕ and elastic constants E_{11}, E_{22}, ν_{12} and G_{12} of the orthotropic layer as

$$[\overline{Q}]_k = [T]_k^{-1} [Q] [T]_k^{-T}. \tag{4-5}$$

The superscript -1 denotes the matrix inverse and -T denotes the transpose of the inverse matrix. The matrix $[T]_k$ is the coordinate transformation matrix and [Q] is the reduced stiffness matrix, given by

$$[T]_k = \begin{bmatrix} \cos^2\phi_k & \sin^2\phi_k & \sin\, 2\phi_k \\ \sin^2\phi_k & \cos^2\phi_k & -\sin\, 2\phi_k \\ -\sin\phi_k \cos\phi_k & \sin\phi_k \cos\phi_k & \cos\, 2\phi_k \end{bmatrix},$$
$$[Q] = \begin{bmatrix} E_{11}/(1-\nu_{12}\nu_{21}) & \nu_{12}E_{22}/(1-\nu_{12}\nu_{21}) & 0 \\ \nu_{12}E_{22}/(1-\nu_{12}\nu_{21}) & E_{22}/(1-\nu_{12}\nu_{21}) & 0 \\ 0 & 0 & G_{12} \end{bmatrix}. \tag{4-6}$$

4.1.2 Bending Stiffness Equivalence

The bending stiffness matrix will now be shown to have an important property: <u>when the stacking sequence is changed, we can always recover the original bending stiffness matrix by appropriately changing layer thicknesses while preserving the total laminate thickness.</u> This property is proved in two steps. First, it is shown that when the ply orientations in two adjacent layers are interchanged, there exists an equivalent design with the same bending stiffness and the same total thickness. Then we show by induction that the same property applies to the general rearrangement of all layers.

Consider a symmetric laminated plate with 2n layers (Fig. 15-a). The elements of the original bending stiffness matrix are given by

$$\begin{aligned} D^a_{ij} = \frac{2}{3}\sum_{k=1}^{\tau-2}(\overline{Q}_{ij})_k(Z^3_k - Z^3_{k+1}) + \frac{2}{3}(\overline{Q}_{ij})_{\tau-1}(Z^3_{\tau-1} - Z^3_{\tau}) + \frac{2}{3}(\overline{Q}_{ij})_{\tau}(Z^3_{\tau} - Z^3_{\tau+1}) \\ + \frac{2}{3}\sum_{k=\tau+1}^{n}(\overline{Q}_{ij})_k(Z^3_k - Z^3_{k+1}) \qquad \text{for } i, j = 1, 2, 6. \end{aligned} \tag{4-7}$$

When the ply orientations in the $\tau - 1$ and τ layers are interchanged (shown in Fig. 15-b), we can still obtain the same D_{ij} by changing the thicknesses of layers $\tau - 1$ and τ. The bending stiffness of the laminate in Fig. 15-b is

$$\begin{aligned} D^b_{ij} = \frac{2}{3}\sum_{k=1}^{\tau-2}(\overline{Q}_{ij})_k(Z^3_k - Z^3_{k+1}) + \frac{2}{3}(\overline{Q}_{ij})_{\tau}(Z^3_{\tau-1} - Z^3_{*}) + \frac{2}{3}(\overline{Q}_{ij})_{\tau-1}(Z^3_{*} - Z^3_{\tau+1}) \\ + \frac{2}{3}\sum_{k=\tau+1}^{n}(\overline{Q}_{ij})_k(Z^3_k - Z^3_{k+1}) \qquad \text{for } i, j = 1, 2, 6. \end{aligned} \tag{4-8}$$

where Z_* is the new height of the bottom of layer τ, determined so that the two plates have the same bending stiffness. Setting $D^a_{ij} = D^b_{ij}$ from Eqs. (4-7) and (4-8), we obtain

$$\{(\overline{Q}_{ij})_\tau - (\overline{Q}_{ij})_{\tau-1}\}\{Z_*^3 - Z_{\tau-1}^3 + Z_\tau^3 - Z_{\tau+1}^3\} = 0 \quad \text{for i, j} = 1, 2, 6. \tag{4 – 9}$$

These equations are satisfied for arbitrary $\overline{Q}$'s if Z_* is chosen such that

$$Z_* = \sqrt[3]{Z_{\tau-1}^3 - Z_\tau^3 + Z_{\tau+1}^3}\,. \tag{4 – 10}$$

Since $Z_{\tau-1} \geq Z_\tau \geq Z_{\tau+1}$, $Z_{\tau+1}^3 - Z_\tau^3 \leq 0$ and, from Eq. (4-10), $Z_* \leq Z_{\tau-1}$. Similarly, $Z_{\tau-1}^3 - Z_\tau^3 \geq 0$ so that $Z_* \geq Z_{\tau+1}$. Hence the height Z_* always falls between $Z_{\tau-1}$ and $Z_{\tau+1}$. This shows that there always exists a design producing the same bending stiffness matrix [D] when ply orientations in two adjacent layers are interchanged.

The general results for interchanging ply orientations in any number of layers follows by induction, because a general interchange is a sequence of transpositions. For example, an equivalent design for a $(45°/90°/0°)_s$ laminate can be obtained from a $(0°/90°/45°)_s$ laminate using three transpositions and thicknesses recomputed by Eq. (4-10). First, we obtain an equivalent design for a $(90°/0°/45°)_s$ laminate from the $(0°/90°/45°)_s$ laminate, then a $(90°/45°/0°)_s$ laminate is obtained from the $(90°/0°/45°)_s$ laminate, and finally the $(45°/90°/0°)_s$ laminate is obtained from the $(90°/45°/0°)_s$.

It should be noted that the above transformation changes the individual thicknesses of the original laminate. Therefore the membrane stiffness is changed, while the bending stiffness remains the same. The existence of multiple laminate designs with the same total thickness and the same bending stiffness has important implications for the optimization process in that it results in multiple optima, as will be shown in the next example.

4.2 Optimal Plate Designs

The plate we consider is simply supported along all four edges and subject to uniform in-plane loading in the X-direction, as shown in Fig. 16. The dimensions of the plate in the X and Y directions are a and b, respectively. Half the thickness of the plate is denoted by T_T and is considered small in comparison with the other dimensions. Shear deformation is not considered in the analysis.

4.2.1 Optimization Problem

The optimization problem that we consider here is to maximize the buckling load of a plate for a given total plate thickness. The thickness of each layer is assumed to be constant over the plate, and for a given stacking sequence of the layers, each thickness is taken as a design variable. Here we use nondimensional values for the plate dimensions and the buckling load. Details of the nondimensional process are given in the next chapter, section 5.1.1.

The nondimensional thicknesses, t_i, are subject to bound constraints

$$t_{min} \leq t_i \leq t_{max} \qquad \text{for } i = 1, \ldots, n, \qquad (4-11)$$

where t_{max} and t_{min} are upper and lower bounds, respectively.

The optimization problem is written as

$$\max_{t_i} \quad n_x \qquad (4-12)$$

such that $\sum_{i=1}^{n} t_i - t_T = 0$

and $t_{min} \le t_i \le t_{max}$ for $i = 1, \ldots, n$,

where n_x is the nondimensional buckling load and t_T is the nondimensional value of T_T (half the thickness of the plate).

4.2.2 Results and Discussion

Some examples are presented to demonstrate the effect of optimization of layer thicknesses on the buckling of laminated plates. A graphite/epoxy composite plate is selected and its material properties are given by $E_{11} = 21.374 \times 10^{10}$ pa (31.0×10^6 psi), $E_{22} = 2.334 \times 10^{10}$ pa (3.4×10^6 psi), $G_{12} = 0.517 \times 10^{10}$ pa (0.75×10^6 psi), and $\nu_{12} = 0.28$, corresponding to nondimensional properties $e_{22} = 0.1097$, $g_{12} = 0.02419$. The plate aspect ratio (l_1/l_2) is chosen to be 1.2.

The solution process of Problem (4-12) and the complete results for $(0°/90°/45°)_s$ and $(45°/90°/0°)_s$ laminates are presented in the next chapter, sections 5.1.2 - 5.1.5.

Results for these examples show that the optimum designs at $t_T = 1.0$ give the same buckling loads ($n_x = 16.232$) for both $(0°/90°/45°)_s$ and $(45°/90°/0°)_s$ laminates. The operation described in section 4.1.2 enables us to obtain a $(45°/90°/0°)_s$ design transforming from a $(0°/90°/45°)_s$ design with the same stiffness matrix and the same total thickness. In fact, there are six possible stacking sequences for this case. Designs for all five other sequences were obtained from the $(0°/90°/45°)_s$ design using Eq. (4-10) and the results are summarized in Table 4. The thickness distribution of the $(45°/90°/0°)_s$ laminate matches the result obtained from the optimization procedure, as it must. The buckling loads for all six designs are the same. Their relationships to the buckling loads for the plate with equal thicknesses are given in the last column of Table 4. In transforming to an equivalent design we assume all the design variables for both designs are free from the bound constraints.

In practical design, the thickness of each layer can take only discrete values due to manufacturing requirements. For example, assume that there is a total of 50 plies in the laminate so that each layer is made up from laminas of nondimensional thickness 0.04. The optimal thicknesses from Table 4 are rounded off to the nearest multiple of 0.04. If this leads to a total thickness which is not unity, we modify one of the thickness such that the percentage change from the continuous solution is minimal. The results are presented in Table 5. It is seen that the buckling loads for all six laminates are within 1% of each other and are close to the previous optimal value $n_x = 16.232$.

The existence of equivalent designs with various stacking sequences has two important implications in terms of multiplicity of optimal designs. First, when an optimum design for a given stacking sequence is obtained, all the designs (with the same total thickness and bending stiffnesses) obtained by permuting the stacking sequences are also optimum. This can be proven as follows: If there is another design for a rearranged stacking sequence which has a higher buckling load than the transformed design, a backward transformation should give a design which has a higher buckling load than the optimum design for the original stacking sequence. This is impossible, so the transformed design is also optimum. In fact, the results in Table 4 were verified to be optimum by direct optimization.

Second, for a given stacking sequence, when two or more layers have the same ply orientation, the optimum design is not unique. For example, consider a four-layer $(45°/0°/45°/90°)_s$ laminate with thicknesses t_1, t_2, t_3, and t_4. We can exchange the 0° and 45° layers to get a $(45°/45°/0°/90°)_s$ design with thicknesses t_1, t_2', t_3', t_4, and then change the division between the two adjacent 45° layers. For example, we can redefine the thicknesses as $\frac{1}{2}t_1$, $\frac{1}{2}t_1 + t_2'$, t_3', t_4. Finally, we can switch the adjacent 45° and 0° layers to get a $(45°/0°/45°/90°)_s$ laminate with thicknesses $\frac{1}{2}t_1$, t_2'', t_3'', t_4 , which has the same stacking sequence, the same buckling load and the same total thickness as the original design (so that it is also optimum), but different individual thicknesses.

We reiterate that these properties assume that the thicknesses are not equal to one of their bounds, and that the plate behavior is governed by Eqs. (4-1) and (4-2) so the membrane stiffnesses are not included.

Stacking sequence of lamina	Reference plate	z_{r+1}	z_r	z_{r-1}	z_*	t_1	t_2	t_3	R[1]
$(0°/90°/45°)_s$	-	-	-	-	-	0.0366	0.1539	0.8095	1.38
$(0°/45°/90°)_s$	$(0°/90°/45°)_s$	0.	0.8095	0.9634	0.7139	0.0366	0.2496	0.7139	1.31
$(45°/0°/90°)_s$	$(0°/45°/90°)_s$	0.7139	0.9634	1.0	0.7772	0.2228	0.0634	0.7139	1.12
$(45°/90°/0°)_s$	$(45°/0°/90°)_s$	0.	0.7139	0.7772	0.4729	0.2228	0.3044	0.4729	1.03
$(90°/45°/0°)_s$	$(45°/90°/0°)_s$	0.4729	0.7772	1.0	0.8601	0.1399	0.3872	0.4729	1.32
$(90°/0°/45°)_s$	$(90°/45°/0°)_s$	0.	0.4729	0.8601	0.8095	0.1399	0.0506	0.8095	1.17

[1] R is the ratio of the optimal buckling load to the buckling load when $t_1 = t_2 = t_3 = 1/3$.

Table 4. Equivalent optimum designs obtained by permutation of stacking sequence (t_t = 1.0)

Table 5. Nondimensional buckling loads for 6 optimal laminates with integer number of plies

Stacking sequence of lamina	t_1	t_2	t_3	n_x
$(0°/90°_4/45°_{20})_s$	0.04	0.16	0.80	16.21
$(0°/45°_6/90°_{18})_s$	0.04	0.24	0.72	16.21
$(45°_5/0°_2/90°_{18})_s$	0.20	0.08	0.72	16.09
$(45°_5/90°_8/0°_{12})_s$	0.20	0.32	0.48	16.05
$(90°_3/45°_{10}/0°_{12})_s$	0.12	0.40	0.48	16.10
$(90°_3/0°/45°_{21})_s$	0.12	0.04	0.84	16.19

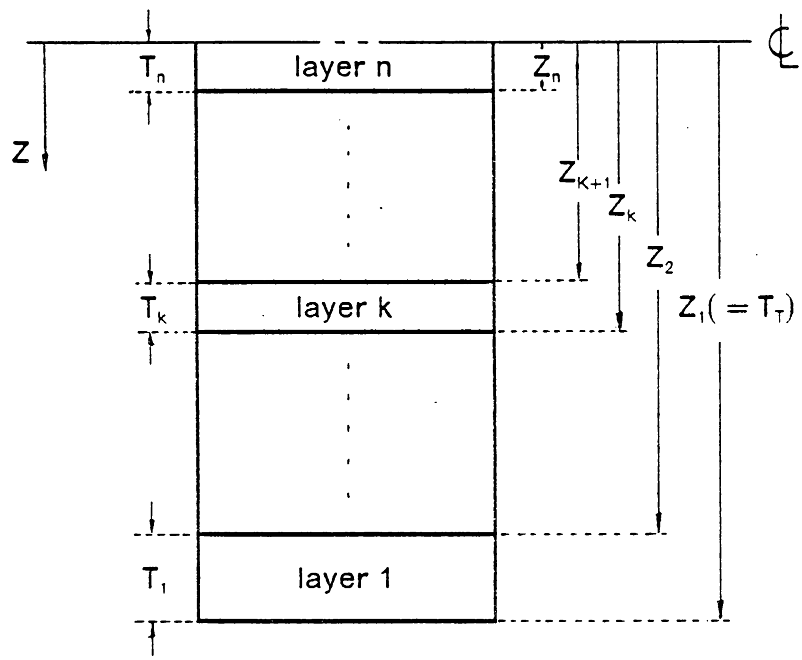

Figure 14. Geometry of Half of a 2n-layered Symmetric Laminate

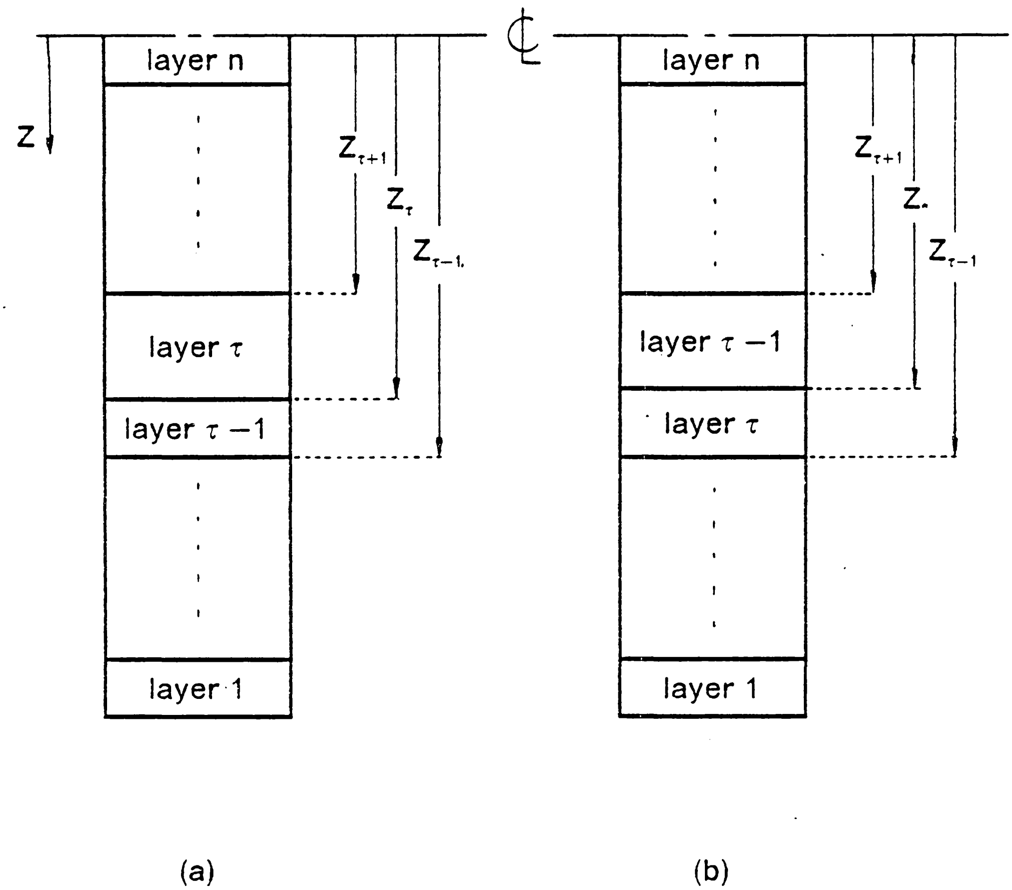

Figure 15. Symmetric 2n-layered Laminates

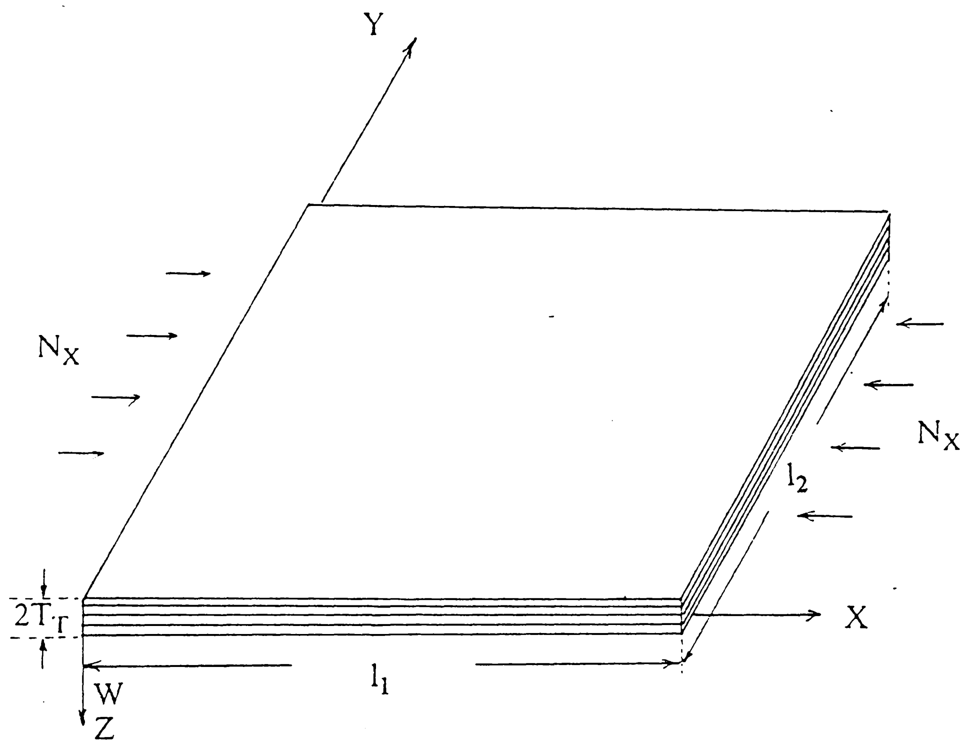

Figure 16. Geometry of Plate Under Uniform Uniaxial In-plane Load

Chapter 5

Sequential Nested Approach

In Chapter 3, the homotopy optimization method was formulated using a simultaneous approach. In this chapter, we apply the method with the more traditional sequential approach. Here the buckling equation is solved separately from the optimality equations. The procedure is applied to two examples; the design of unstiffened laminated plates and the design of stiffened laminated plates.

5.1 Design of Unstiffened Laminate Plates

The same plate model from the previous chapter is used for this study. It is simply supported along all four edges and subject to uniform in-plane loading in the X-direction, as shown in Fig. 16.

5.1.1 Buckling Analysis

The differential equation for the buckling analysis is given by

$$\frac{\partial^2 M_X}{\partial X^2} + 2\frac{\partial^2 M_{XY}}{\partial X \partial Y} + \frac{\partial^2 M_Y}{\partial Y^2} - N_X \frac{\partial^2 W}{\partial X^2} = 0, \tag{5-1}$$

where N_X is the buckling load and W denotes the transverse deflection of the middle surface of the plate. The moments are given in Eq. (4-1).

The analysis is performed with dimensionless quantities. First, using the nondimensional material properties,

$$e_{22} = \frac{E_{22}}{E_{11}}, \qquad g_{12} = \frac{G_{12}}{E_{11}}, \tag{5-2}$$

the nondimensional reduced stiffness matrix is

$$[\overline{q}]_k = \frac{1}{E_{11}}[\overline{Q}]_k = [T]_k^{-1}\begin{bmatrix} 1/(1-\nu_{12}\nu_{21}) & \nu_{12}e_{22}/(1-\nu_{12}\nu_{21}) & 0 \\ \nu_{12}e_{22}/(1-\nu_{12}\nu_{21}) & e_{22}/(1-\nu_{12}\nu_{21}) & 0 \\ 0 & 0 & g_{12} \end{bmatrix}[T]_k^{-T}. \tag{5-3}$$

Quantities relating to plate thickness such as Z_i, T_T, and T_i are normalized by T_{Tmax}, the maximum total thickness considered in the optimization study:

$$z_i = \frac{Z_i}{T_{Tmax}}, \qquad t_T = \frac{T_T}{T_{Tmax}}, \qquad t_i = \frac{T_i}{T_{Tmax}}. \tag{5-4}$$

Substituting Eqs. (5-3) and (5-4) into Eq. (4-4) in the previous chapter, we obtain the nondimensional laminate stiffness matrix

$$[d] = \frac{1}{E_{11}T^3_{Tmax}}[D] = \frac{2}{3}\sum_{k=1}^{n}[q]_k\,(z_k^3 - z_{k+1}^3). \tag{5-5}$$

The coordinates and displacements are nondimensionalized by the plate length in the x-direction, l_1:

$$x = \frac{X}{l_1}, \qquad y = \frac{Y}{l_1}, \qquad w = \frac{W}{l_1}, \tag{5-6}$$

and the nondimensional moments, m_x, m_y, and m_{xy} are defined as

$$\begin{Bmatrix} m_x \\ m_y \\ m_{xy} \end{Bmatrix} = \frac{l_1}{E_{11}T^3_{Tmax}}\begin{Bmatrix} M_X \\ M_Y \\ M_{XY} \end{Bmatrix} = [d]\begin{Bmatrix} -\frac{\partial^2 w}{\partial x^2} & -\frac{\partial^2 w}{\partial y^2} & -2\frac{\partial^2 w}{\partial x \partial y} \end{Bmatrix}^T. \tag{5-7}$$

Finally, using Eqs. (5-6) and (5-7) the original buckling differential equation is transformed to

$$\frac{\partial^2 m_x}{\partial x^2} + 2\frac{\partial^2 m_{xy}}{\partial x \partial y} + \frac{\partial^2 m_y}{\partial y^2} - n_x\frac{\partial^2 w}{\partial x^2} = 0, \tag{5-8}$$

where n_x is the nondimensional buckling load defined by

$$n_x = \frac{l_1^2}{E_{11}T^3_{Tmax}} N_X. \tag{5-9}$$

The differential equation is solved by the finite element method using a 16-degree-of-freedom element first introduced by Bogner, Fox, and Schmit [52].

Assuming the in-plane load is uniform, the finite element discretization of Eq. (5-8) is

$$[K]\{U\} - n_x[K_G]\{U\} = 0, \tag{5-10}$$

where [K] is the system stiffness matrix, $[K_G]$ is the system geometric stiffness matrix, and $\{U\}$ is the buckling mode. The above matrix equation is solved using SNLASO, one of the subroutines from the package LASO2 [53], which computes a few eigenvalues and the associated eigenvectors of a large (sparse) symmetric matrix using the Lanczos algorithm [54].

The optimization procedure requires derivatives of the buckling load with respect to the thickness variables t_i. These are calculated explicitly by differentiating the Rayleigh quotient associated with Eq. (5-10):

$$\frac{dn_x}{dt_i} = \frac{\{U\}^T \dfrac{\partial[K]}{\partial t_i} \{U\}}{\{U\}^T [K_G] \{U\}} . \tag{5-11}$$

The stiffness matrix derivatives, $\dfrac{\partial[K]}{\partial t_i}$, are estimated by forward finite difference approximations.

Sometimes the optimum design is bimodal, in which case there are two eigenvectors corresponding to the lowest eigenvalue. The buckling load is not differentiable for this case. To eliminate this difficulty, we use a constraint, $n_{x1} = 0.999\, n_{x2}$ in the bimodal formulation (see section 5.1.3) so that the buckling modes can be determined separately for the first buckling load, n_{x1} , and the second buckling load, n_{x2} .

5.1.2 Optimization Problem

The optimization problem that we consider here is to maximize the buckling load of a plate for a given total plate thickness. The thickness of each layer is assumed to be constant over the plate, and for a given stacking sequence of the layers, each thickness is taken as a design variable. The nondimensional thicknesses, t_i, are subject to bound constraints

$$t_{min} \le t_i \le t_{max} \qquad \text{for } i = 1, \ldots, n, \tag{5-12}$$

where t_{max} and t_{min} are upper and lower bounds, respectively.

The optimization problem is written as

$$\max_{t_i} \quad n_x \tag{5-13}$$

$$\text{such that} \quad \sum_{i=1}^{n} t_i - t_T = 0$$

$$\text{and} \quad t_{min} \le t_i \le t_{max} \qquad \text{for } i = 1, \ldots, n,$$

where the nondimensional buckling load, n_x, is obtained by solving Eq. (5-10).

The problem (5-13) can be solved using the homotopy technique described in section 3.2. The total thickness of the plate, t_T , is chosen as the homotopy parameter, and for the initial conditions for the initial value problem we use the minimum-thickness plate with t_T corresponding to all design variables at their lower bound. The trajectory of the initial value problem is a path of optima corresponding to varying t_T.

The equations defining the path of optimal designs are obtained using Lagrange multipliers. The optimum path consists of several smooth segments, with breaks in smoothness at points where the active constraint set changes. Following the same discussion in the section 3.1.1, we can set the active inequality constraints as equality constraints,

$$t_j = t_{min} \quad \text{or} \quad t_j = t_{max} \qquad \text{for } j \in I_A, \tag{5-14}$$

where I_A is the set of indices of thicknesses which are at a lower or upper bound. These variables are eliminated from the optimization problem, while the other variables are left unconstrained. The optimization problem along a segment can, therefore, be written as

$$\max_{t_i} \quad n_x \qquad \text{for } i \notin I_A \tag{5-15}$$

$$\text{such that} \quad \sum_{i=1}^{n} t_i - t_T = 0. \tag{5-16}$$

5.1.3 Stationary Conditions

Using a Lagrange multiplier μ, the augmented function $n_x{}^*$ is

$$n_x{}^* = n_x - \mu[\sum_{i=1}^{n} t_i - t_T]. \tag{5-17}$$

Taking the first derivatives of $n_x{}^*$ with respect to t_i and μ, and setting them equal to zero, we obtain the optimality conditions

$$\frac{\partial n_x}{\partial t_i} - \mu = 0 \qquad \text{for } i \notin I_A \tag{5-18}$$

and the total thickness constraint of Eq. (5-16). Equations (5-16) and (5-18) form a system of nonlinear equations to be solved for t_i and μ. A homotopy method is used to find the solution of these equations for varying t_T.

The stationary conditions for bimodal solutions are obtained by adding a bimodality constraint into the augmented function in Eq.(5-17). Then we have

i) Optimality conditions

$$(1-\gamma)\frac{\partial n_{x1}}{\partial t_i} + 0.999\,\gamma\,\frac{\partial n_{x2}}{\partial t_i} - \mu = 0 \qquad \text{for } i \notin I_A \tag{5-19}$$

ii) Bimodality constraint

$$n_{x1} - 0.999\, n_{x2} = 0 \tag{5-20}$$

and the total thickness constraint of Eq. (5-16). In Eq. (5-19), γ denotes the Lagrange multiplier of the bimodality constraint.

5.1.4 Tracing Optima

There are four types of transitions as was described in Section 3.3:

Type 1: A bound constraint becoming active (i.e., being satisfied as an equality);

Type 2: A bound constraint becoming inactive;

Type 3: Transition from a unimodal solution to a bimodal solution;

Type 4: Transition from a bimodal solution to a unimodal solution.

Transition points of type 1 are located by checking the bound constraints (5-12).

Transition points of type 2 are detected by checking positivity of all Lagrange multipliers for bound constraints. These multipliers are obtained by replacing the augmented function n_x^* (for the unimodal case) in Eq. (5-17) by

$$n_x{}^* = n_x - \mu[\sum_{i=1}^{n} t_i - t_T] - \sum_{i\in I_A} \lambda_{1i}[t_{min} - t_i] - \sum_{i\in I_A} \lambda_{2i}[t_i - t_{max}]. \qquad (5-21)$$

Taking the first derivatives of $n_x{}^*$ with respect to t_i and setting them equal to zero, we obtain

$$\frac{\partial n_x}{\partial t_i} - \mu + \lambda_{1i} - \lambda_{2i} = 0 \qquad \text{for } i \in I_A. \qquad (5-22)$$

Since $\lambda_{1i} = 0$ for $t = t_{max}$ and $\lambda_{2i} = 0$ for $t = t_{min}$, λ_{1i} and λ_{2i} are given by

$$\begin{aligned} \lambda_{1i} &= -\frac{\partial n_x}{\partial t_i} + \mu \qquad &\text{for } t_i = t_{min} \\ \lambda_{2i} &= \frac{\partial n_x}{\partial t_i} - \mu \qquad &\text{for } t_i = t_{max}. \end{aligned} \qquad (5-23)$$

Similar equations for the bimodal case are as follows.

$$\begin{aligned} \lambda_{1i} &= -(1-\gamma)\frac{\partial n_{x1}}{\partial t_i} - 0.999\,\gamma\,\frac{\partial n_{x2}}{\partial t_i} + \mu \qquad &\text{for } t_i = t_{min} \\ \lambda_{2i} &= (1-\gamma)\frac{\partial n_{x1}}{\partial t_i} + 0.999\,\gamma\,\frac{\partial n_{x1}}{\partial t_i} - \mu \qquad &\text{for } t_i = t_{max}. \end{aligned} \qquad (5-24)$$

A transition of type 3 occurs when two buckling loads approach together and meet, as shown in Fig. 17. Optimal designs become bimodal for the subsequent segment on the solution path. The homotopy routine traces solutions on a smooth path using sensitivity information obtained from the previous point. To preserve the smoothness of the solution path, the tracing routine picks at each step the eigenvalue n_x corresponding to the critical n_x in the previous step. As soon as the transition is passed this n_x is no longer the lowest one, and this event identifies transition type 3.

The bimodal formulation includes an additional constraint for the bimodality requirement, and this constraint is handled with a Lagrange multiplier γ. The following inequality is necessary in the bimodal range and can be used to detect the type 4 transition from bimodal to unimodal:

$$0 \leq \gamma \leq 1. \tag{5-25}$$

At a transition point there are a number of solution paths which satisfy the stationary equations, so we need to choose a path which satisfies the optimality conditions. Choosing an optimum path constitutes finding a set of active bound constraints for type 1 and 2 transitions and the correct buckling modes for type 3 and 4 transitions. This procedure was explained in section 3.3.2.

5.1.5 Results and Discussion

Some examples are presented to demonstrate the effect of optimization of layer thicknesses on the buckling of laminated plates. A graphite/epoxy composite plate is selected and its material properties are given by $E_{11} = 21.374\text{x}10^{10}$ pa ($31.0\text{x}10^6$ psi), $E_{22} = 2.334\text{x}10^{10}$ pa ($3.4\text{x}10^6$ psi), $G_{12} = 0.517\text{x}10^{10}$ pa ($0.75\text{x}10^6$ psi), and $\nu_{12} = 0.28$, corresponding to nondimensional properties $e_{22} = 0.1097$, $g_{12} = 0.02419$. The plate aspect ratio (l_1/l_2) is chosen to be 1.2.

To determine an appropriate mesh size for the finite element analysis, a series of numerical tests were performed for a $(0°/90°/45°)_s$ laminate. The nondimensional thickness of each layer was set at 1/3. Table 6 shows the first and second buckling loads for different meshes. The first buckling load is quite accurate even for a 2x2 mesh (less than 1 % difference compared to the 6x6 mesh); however, the second buckling load, which has a full sine mode in the x-direction, converges more slowly as the mesh is refined. Since the optimum designs are often bimodal, the first two buckling loads must be considered in the analysis, and a 4x4 mesh is chosen for the finite element analysis.

First, optimization results are presented for this $(0°/90°/45°)_s$ laminate for which the thickness of each layer is taken as a design variable. This laminate consists of six layers; however, only three of them are treated as design variables due to symmetry. The nondimensional minimum gage,

t_{min}, is set at 0.01, so the design starts from $t_T = 0.03$ where all design variables are at the minimum gage.

Figure 18 shows the nondimensional height of each layer of the optimum design (above the middle surface) obtained for $0.03 \leq t_T \leq 0.3$. The thickness of each layer is the distance between the two adjacent heights. In Fig. 18, each curve has three transition points and consists of four solution segments. The circles on the curves indicate the transition points and the dots are the solutions traced along the optimum path. Along the first two segments ($0.03 \leq t_T \leq 0.185$), the optimum designs are unimodal, and along the last two segments ($0.185 \leq t_T \leq 0.3$), the optimum designs are bimodal. Along the first segment, only one layer (corresponding to the 45° fibers) varies its thickness, along the second and the third segments two layers (90° and 45°) vary, and along the last segment all three layers change thickness. In Fig. 19, the nondimensional buckling loads, n_x, corresponding to these optimum designs are shown in semi-log scale for the same range of t_T. The dashed line indicates the buckling loads of reference designs in which all layers have the same thickness. Once all design variables are above their minimum gages ($t_T \geq 0.274$) we reach the optimum unconstrained ratios of layer thicknesses. These optimum ratios are preserved as we increase the total thickness of the plate, t_T . Above $t_T = 0.274$ the design variables are increased proportionally to t_T, the buckling load is proportional to t_T^3, and the set of active constraints is fixed. Therefore, there is no need to trace the optimal path beyond $t_T = 0.274$.

Next, a $(45°/90°/0°)_s$ laminate is considered. Figure 20 shows the height of each layer of the optimum design for $0.03 \leq t_T \leq 0.05$ and Fig. 21 shows the corresponding nondimensional buckling loads. This path has two transition points and consists of three solution segments. Along the first segment $0.03 \leq t_T \leq 0.0337$ the optimum designs are unimodal, and along the last two segments the optimum designs are bimodal. Along the first segment, only the 0° layer varies its thickness, along the second segment two layers (90° and 0°) vary, and along the last segment ($t_T \geq 0.0449$) all three layers change thickness. The nondimensional buckling load at $t_T > 0.0449$ is obtained by scaling the buckling load at $t_T = 0.0449$ by $(t_T/0.0449)^3$.

5.2 Design of Laminated Plate with a Stiffener

The plate model in this section has a symmetric blade stiffener at center as shown in Fig. 22. Again the plate is simply supported along all four edges.

5.2.1 Buckling Analysis

The analysis of the stiffened plate is performed in two steps for the finite element analysis. First, the stiffener at the center is treated as a beam in forming the global stiffness matrix. Then, the local buckling of the stiffener is considered separately from the main finite element analysis.

Overall Plate Buckling Analysis

The governing differential equation for the beam stiffener is

$$(E_{11b}I_bW'')'' + P_bW'' = 0 \qquad (5-26)$$

where $''$ denotes $\frac{d^2}{dX^2}$ and P_b is the beam axial load. I_b is the moment of inertia of the beam given by

$$I_b = \frac{2}{3}B\{(H + T_T)^3 - T_T^3\} \qquad (5-27)$$

where B is the width, H is the height of the stiffener and T_T is half the total thickness of the laminate plate (see Fig. 22). Using nondimensional quantities

$$
\begin{aligned}
&b=\frac{B}{l_1}, \quad h=\frac{H}{l_1}, \quad t_T=\frac{T_T}{l_1}, \quad I_b=i_b l_1^4=\frac{2}{3}\,b\{(h+t_T)^3-t_T^3\} \\
&e_{11b}=\frac{E_{11b}}{E_{11}}, \quad w=\frac{W}{l_1}, \quad x=\frac{X}{l_1}, \quad p_b=\frac{1}{E_{11}l_1^2}\,P_b
\end{aligned}
\tag{5-28}
$$

we get the differential equation in nondimensional form:

$$(e_{11b}i_b w'')''+p_b w''=0 \tag{5-29}$$

Nondimensional buckling analysis for the plate is obtained replacing Eq. (5-4) in the Section 5.1.1 by

$$z_i=\frac{Z_i}{l_1}, \qquad t_i=\frac{T_i}{l_1}. \tag{5-30}$$

Then we have

$$n_x=\frac{1}{E_{11}l_1}\,N_X. \tag{5-31}$$

The overall buckling equation in matrix form is

$$[K]\{U\}+[K]_b\{U\}-n_x[K_G]\{U\}-p_b[K_G]_b\{U\}=0, \tag{5-32}$$

where $[K]$ and $[K]_b$ are the plate and the beam stiffness matrices, respectively, $[K_G]$ and $[K_G]_b$ are the plate and the beam geometric stiffness matrices, respectively, and $\{U\}$ is the buckling mode. The total load on the stiffened plate P is distributed as pg_1 to the plate and pg_2 to the stiffener, where

$$
\begin{aligned}
g_1&=\frac{l_2}{l_1}\,\frac{e_p s_p}{e_p s_p+s_b e_b}\\
g_2&=\frac{e_b s_b}{e_p s_p+s_b e_b}
\end{aligned}
\tag{5-33}
$$

where s_p and s_b are the nondimensional cross- sectional area of plate and beam, respectively, expressed as $s_p=2\,l_2 t_T$ and $s_b=2\,b\,h$. And e_p is the stiffness of the laminated plate given by

$$\frac{1}{e_P} = \frac{a_{22}a_{66} - a_{26}^2}{|[a]|} t_T \qquad (5-34)$$

where [a] is the nondimensional stretching stiffness matrix expressed as $[a] = \frac{2}{3}\sum_{k=1}^{n}[q]_k (z_k - z_{k+1})$.

Equation (5-32) may be written now as

$$[K]\{U\} + [K]_b\{U\} - p(g_1[K_G]\{U\} + g_2[K_G]_b\{U\}) = 0, \qquad (5-35)$$

where $pg_1 = n_x$ and $pg_2 = p_b$.

Local Stiffener Buckling Analysis

The local buckling of the stiffener is analyzed separately from the overall plate analysis. The stiffener is treated as a plate which is simply supported at 3 edges and is free at one edge. Levy's solution [55] was used for this local stiffener buckling load, p_s .

5.2.2 Optimization Problem

The optimization problem is to maximize the buckling load of a plate for a given total plate thickness. The design variables are set as the individual thickness of each layer, the width and the height of the stiffener. Here we denote the width and the height of the stiffener as t; $t_{n+1} = b$, $t_{n+2} = h$. The nondimensional design variables, t_i , are subject to bound constraints

$$t_{i\,min} \leq t_i \leq t_{i\,max} \qquad \text{for } i = 1, 2, \ldots, n+2, \qquad (5-36)$$

where $t_{i\,max}$ and $t_{i\,min}$ are upper and lower bounds, respectively, and n is half the number of layers for the symmetric plate.

The optimization problem is written as

$$\max_{t_i} \quad \beta \tag{5-37}$$

$$\text{such that} \quad p_1 \geq \beta$$
$$p_2 \geq \beta$$
$$p_s \geq \beta$$
$$c^T t - \theta = 0$$
$$\text{and} \quad t_{i\,min} \leq t_i \leq t_{i\,max} \qquad \text{for } i = 1, \dots, n+2,$$

where p_1 and p_2 are the first and the second buckling load, respectively, for the overall plate and p_s is the stiffener buckling load. c is a positive cost vector and θ is the total volume of the structure.

The problem (5-37) can be solved using the homotopy technique described in section 3.2. The total volume of the plate, θ , is chosen as the homotopy parameter.

Following the same discussion in the section 3.1.1, we can set the active inequality constraints as equality constraints,

$$t_j = t_{j\,min} \quad \text{or} \quad t_j = t_{j\,max} \qquad \text{for } j \in I_A, \tag{5-38}$$

where I_A is the set of indices of design variables which are at a lower or upper bound. These variables are eliminated from the optimization problem, while the other variables are left unconstrained. The optimization problem along a segment can, therefore, be written as

$$\max_{t_i} \quad \beta \qquad \text{for } i \notin I_A \tag{5-39}$$

such that $p_1 \geq \beta$

$p_2 \geq \beta$

$p_s \geq \beta$

and $c^T t - \theta = 0$

5.2.3 Stationary Conditions

Using the Lagrange multiplier technique the augmented function $\beta*$ is

$$\beta* = \beta - \gamma_1(\beta + r_1^2 - p_1) - \gamma_2(\beta + r_2^2 - p_2) - \gamma_3(\beta + r_3^2 - p_s) - \mu(c^T t - \theta) \qquad (5-40)$$

where γ_1, γ_2, γ_3, and μ are Lagrange multipliers and r_1, r_2, and r_3 are slack variables. Taking the first derivatives of $\beta*$ with respect to all these variables and setting them equal to zero, we obtain the stationary conditions,

$$1 - \gamma_1 - \gamma_2 - \gamma_3 = 0 \qquad (5-41)$$

$$\gamma_1 \frac{\partial p_1}{\partial t_i} + \gamma_2 \frac{\partial p_2}{\partial t_i} + \gamma_3 \frac{\partial p_s}{\partial t_i} - \mu c_i = 0 \qquad \text{for } i \notin I_A \qquad (5-42)$$

$$p_1 - r_1^2 - \beta = 0 \qquad (5-43)$$

$$-2\gamma_1 r_1 = 0 \qquad (5-44)$$

$$p_2 - r_2^2 - \beta = 0 \qquad (5-45)$$

$$-2\gamma_2 r_2 = 0 \qquad (5-46)$$

$$p_s - r_3^2 - \beta = 0 \qquad (5-47)$$

$$- 2\gamma_3 r_3 = 0 \qquad (5-48)$$

$$\theta - c^T t = 0 \qquad (5-49)$$

These equations form a system of nonlinear equations to be solved for optimal design. The homotopy method is used to find the solution of these equations for varying θ. The slack variables are eliminated from Eqs. (5-43) - (5-48) and these equations are changed to

$$\gamma_1(p_1 - \beta) = 0 \qquad (5-50)$$

$$\gamma_2(p_2 - \beta) = 0 \qquad (5-51)$$

$$\gamma_3(p_s - \beta) = 0 \qquad (5-52)$$

5.2.4 Tracing Optima

Again there are four types of transitions:

Type 1: A bound constraint becoming active (i.e., being satisfied as an equality);

Type 2: A bound constraint becoming inactive;

Type 3: An inequality buckling load constraint becoming active;

Type 4: An inequality buckling load constraint becoming inactive.

Transition points of type 1 are located by checking the bound constraints (5-36).

Transition points of type 2 are detected by checking positivity of all Lagrange multipliers for bound constraints. These multipliers are given by

$$\lambda_{1i} = -\gamma_1 \frac{\partial p_1}{\partial t_i} - \gamma_2 \frac{\partial p_2}{\partial t_i} - \gamma_3 \frac{\partial p_s}{\partial t_i} + \mu c_i \qquad \text{for } t_i = t_{min},$$
$$\lambda_{2i} = \gamma_1 \frac{\partial p_1}{\partial t_i} + \gamma_2 \frac{\partial p_2}{\partial t_i} + \gamma_3 \frac{\partial p_s}{\partial t_i} - \mu c_i \qquad \text{for } t_i = t_{max}. \tag{5-53}$$

A transition of type 3 is detected by checking the buckling load constraints;

$$p_1 \geq \beta,$$
$$p_2 \geq \beta, \tag{5-54}$$
$$p_s \geq \beta.$$

A transition of type 4 is detected by checking if the Lagrange multipliers associated with the buckling load constraints are positive;

$$\gamma_1 \geq 0,$$
$$\gamma_2 \geq 0, \tag{5-55}$$
$$\gamma_3 \geq 0.$$

At a transition point there are a number of solution paths which satisfy the stationary equations, so we need to choose a path which satisfies the optimality conditions. This procedure was explained in section 3.3.2.

5.2.5 Results and Discussion

The graphite/epoxy composite material in this example is the same as the one in the previous example. The plate aspect ratio (l_1/l_2) is 1.2 and the mesh size for the finite element analysis is also 4x4.

Optimization results are presented for the $(0°/90°/45°)_s$ laminate with a stiffener in which 0° and 90° layers are mixed with the same proportion. There are five design variables; three thicknesses of plate layers, width and height of the stiffener. The nondimensional minimum gage, t_{min}, is set at 0.002 for the thickness of each layer and the width of the stiffener, and 0.01 for the height of the stiffener. The total volume of the plate are expressed as $\theta = 2(l_2\sum_{i=1}^{3} t_i + b\,h)$. And the design starts from $\theta = 0.01004$ where all design variables are at the minimum gage.

Figure 23 shows the nondimensional height and the width of the optimum design obtained for $0.01004 \leq \theta \leq 0.010827$. The thicknesses of three layers remain at the minimum gage. Initially the optimum design starts with a unimodal solution. The first buckling load of the plate structure, p_1, is active and the optimal design changes only the height of the stiffener. When the total volume reaches at 0.010072, the local buckling load of the stiffener, p_s, also becomes active and the design changes to bimodal. The width of the stiffener and the height changes at the same time from this point. This transition point is indicated by a circle in the Figure 23 and the dots are the solutions traced along the optimum path.

In Fig. 24, the nondimensional buckling loads β corresponding to these optimum designs are shown for the same range of θ. It is noted that the buckling load is increased by 325% while the total volume is increased only 8%. This shows the efficiency of stiffener in designing plate structures for buckling load.

The homotopy routine stopped tracing the optimal path at $\theta = 0.010827$ due to ill-conditioning of the optimal design problem as the solution approaches a trimodal condition; i.e., $p_1 = p_2 = p_s$. The Lagrange multiplier for the second buckling load constraint, γ_2, is 0 at the second segment of the optimum path (because only p_1 and p_s are active). As we increase the total volume along the segment, the second buckling load, p_2, also approaches to β, so both terms in Eq. (5-51) approach to 0. This causes an ill-conditioned Jacobian matrix of the nonlinear system of equations which homotopy method cannot handle.

Table 6. Comparison of buckling loads for different meshes;$(0°/90°/45°)_s$ laminate with $t_1 = t_2 = t_3 = 1/3$

Mesh	2 x 2	3 x 3	4 x 4	5 x 5	6 x 6
First buckling load	11.800	11.742	11.729	11.725	11.724
Second buckling load	27.196	23.369	23.089	23.000	22.969

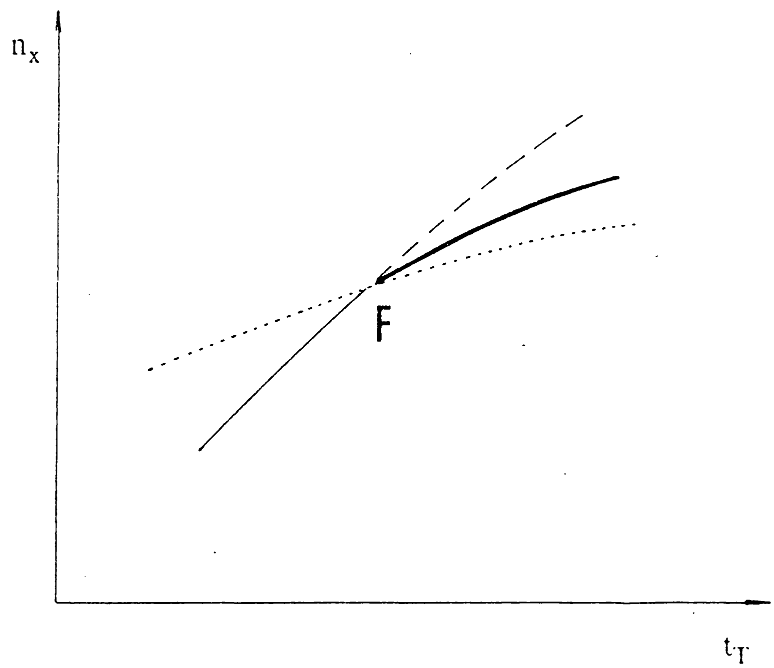

F : Transition point

——— : Path corresponding to mode 1 (Optimum unimodal path)

·········· : Path corresponding to mode 2

– – – – : Artificial path for mode 1

▬▬▬ : Optimum bimodal path

Figure 17. Transition from Unimodal to Bimodal Segment

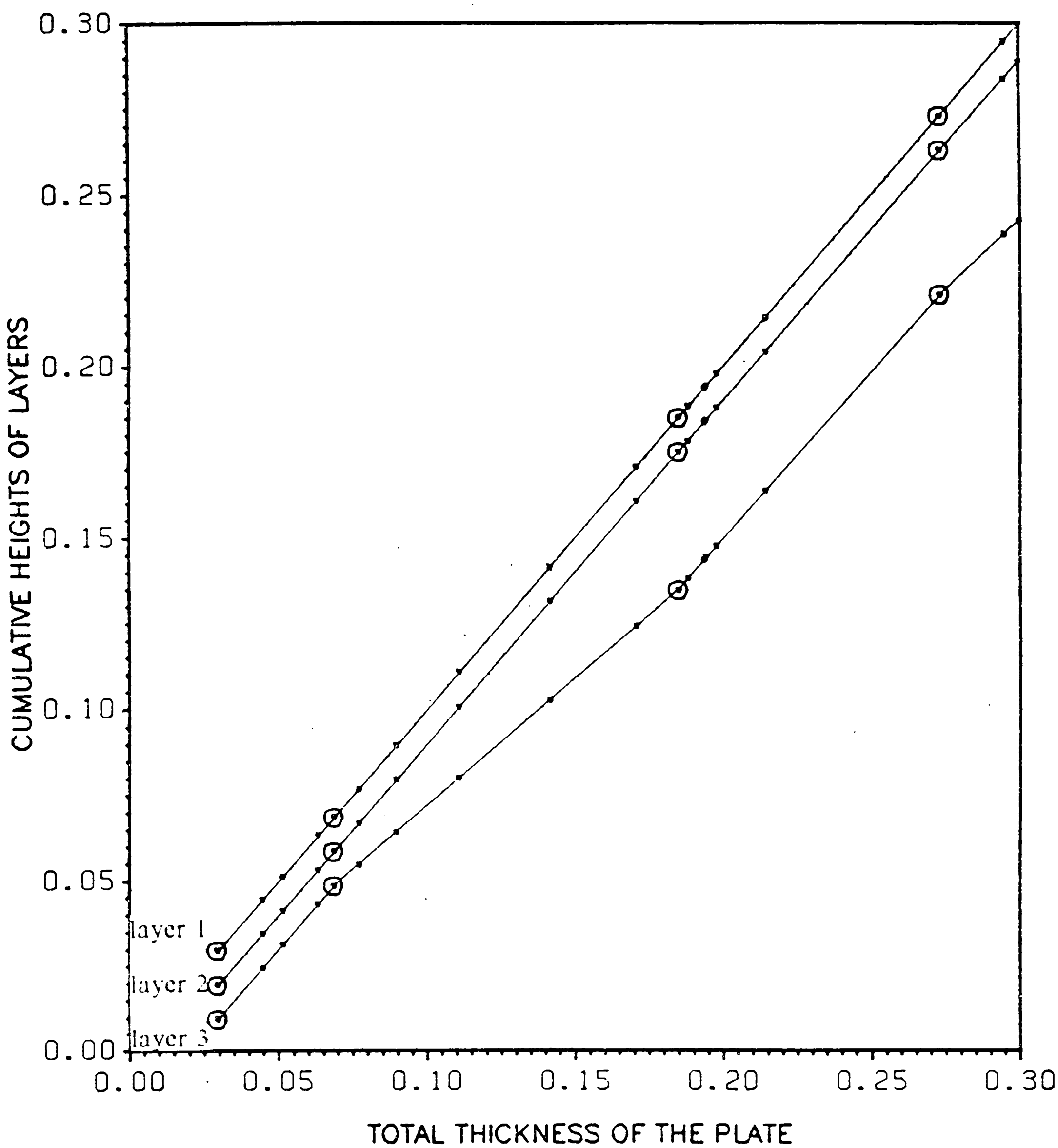

Figure 18. Optimum Thickness Distributions for $(0°/90°/45°)_s$ laminates

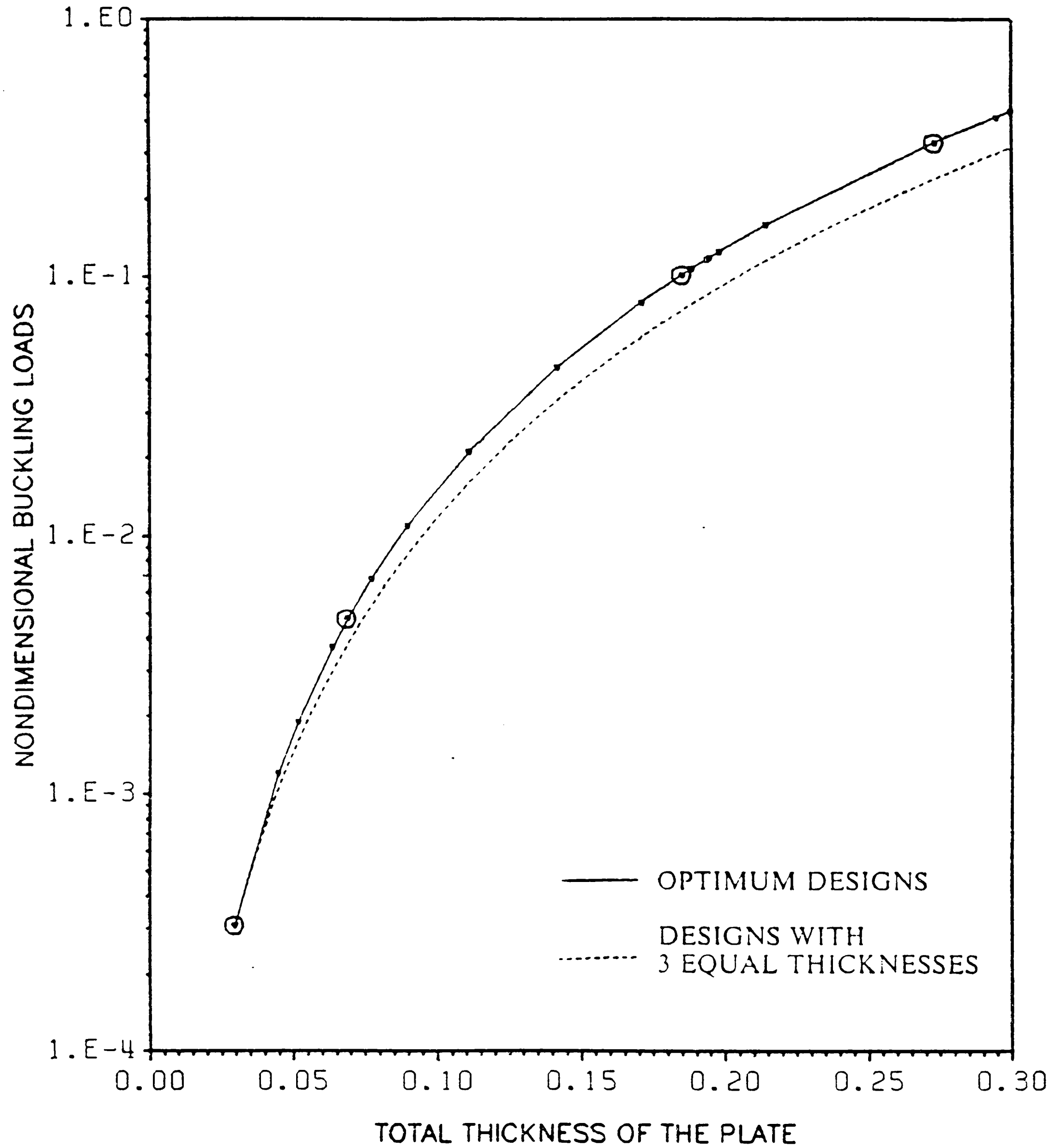

Figure 19. Buckling Loads for Optimum and Equal Thickness $(0°/90°/45°)_s$ laminates

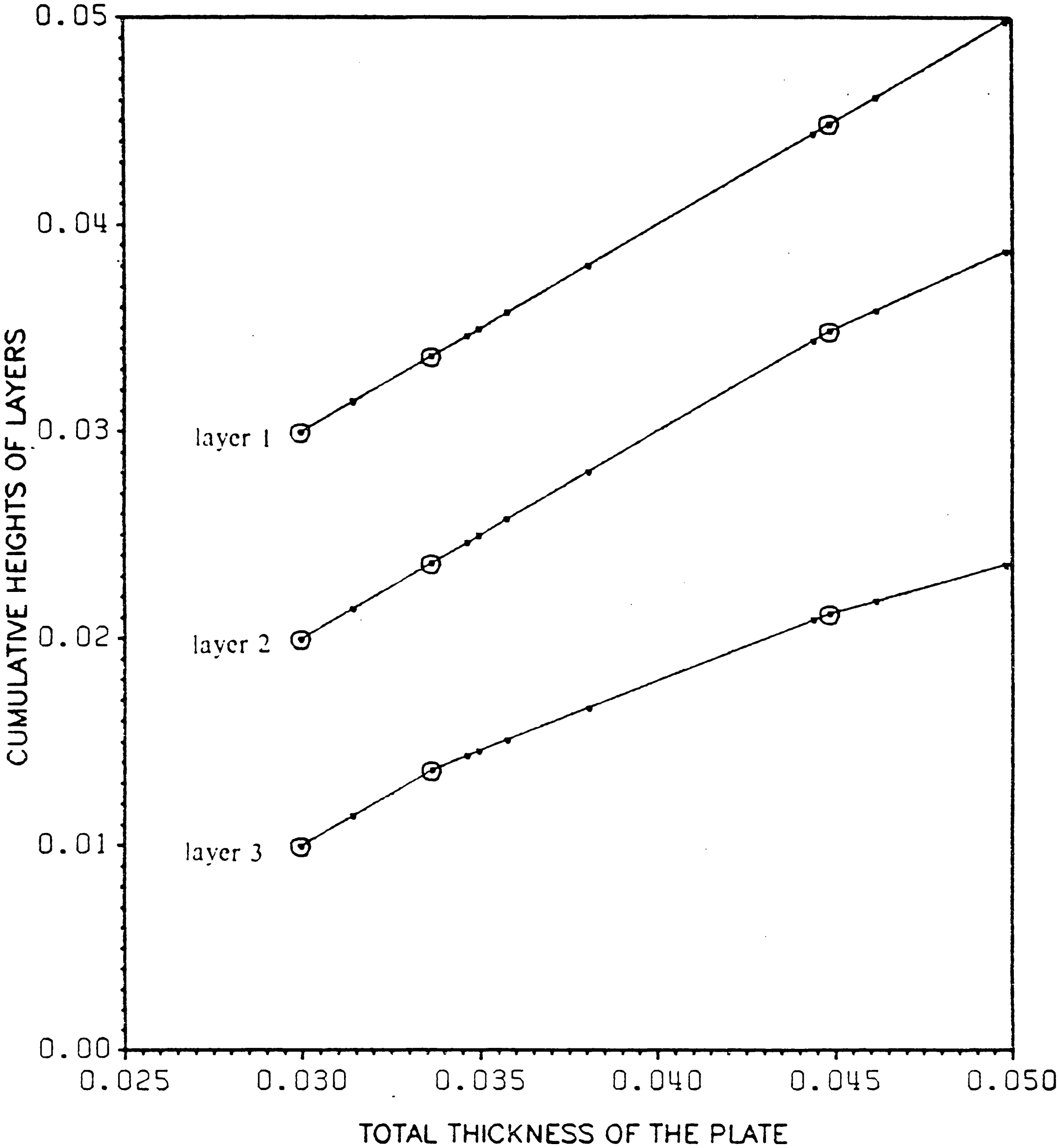

Figure 20. Optimum Thickness Distributions for $(45°/90°/0°)_s$ laminates

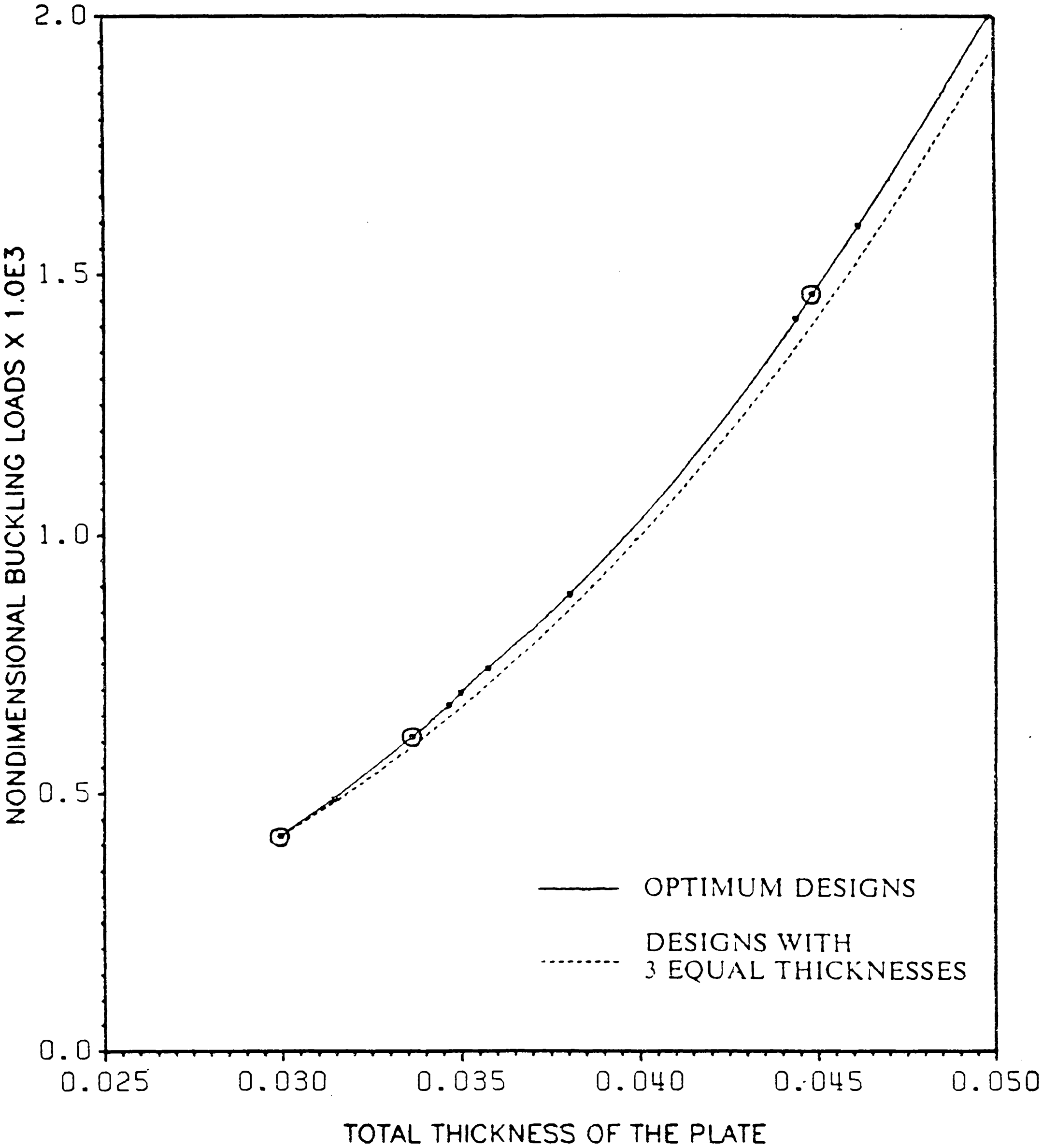

Figure 21. Buckling Loads for Optimum and Equal Thickness $(45°/90°/0°)_s$ laminates

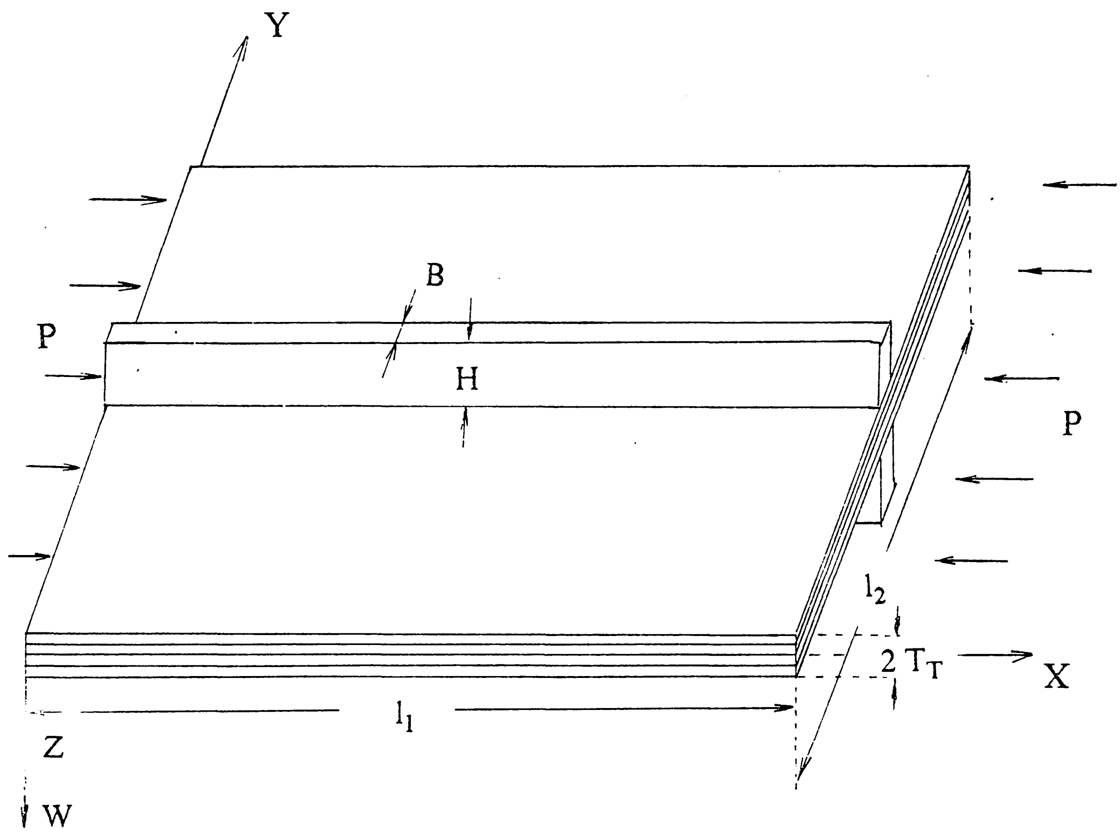

Figure 22. Geometry of Stiffened Plate Under Uniform Uniaxial In-plane Load

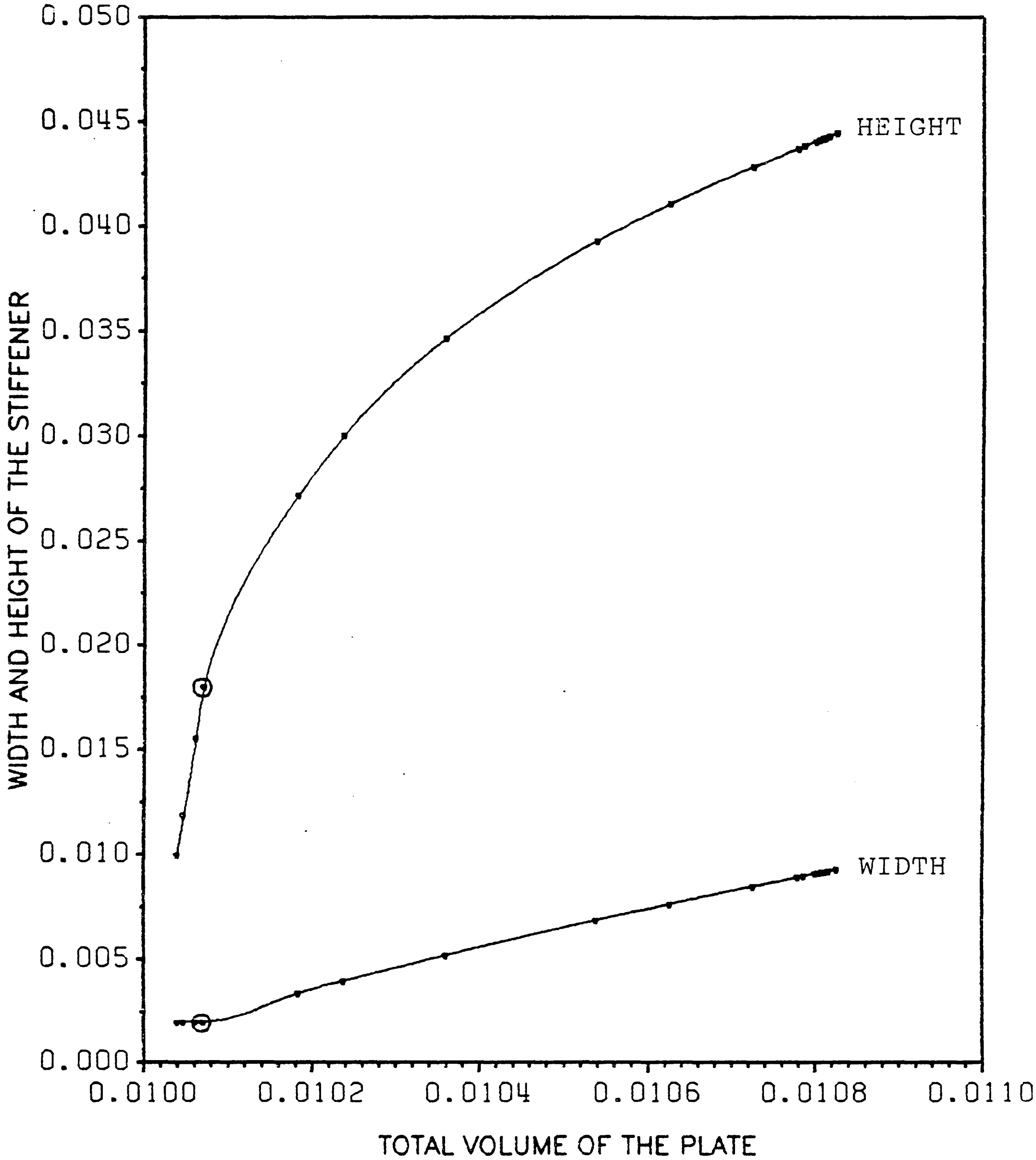

Figure 23. Nondimensional Width and Height of Stiffener for Optimum $(0°/90°/45°)_s$ stiffened laminates

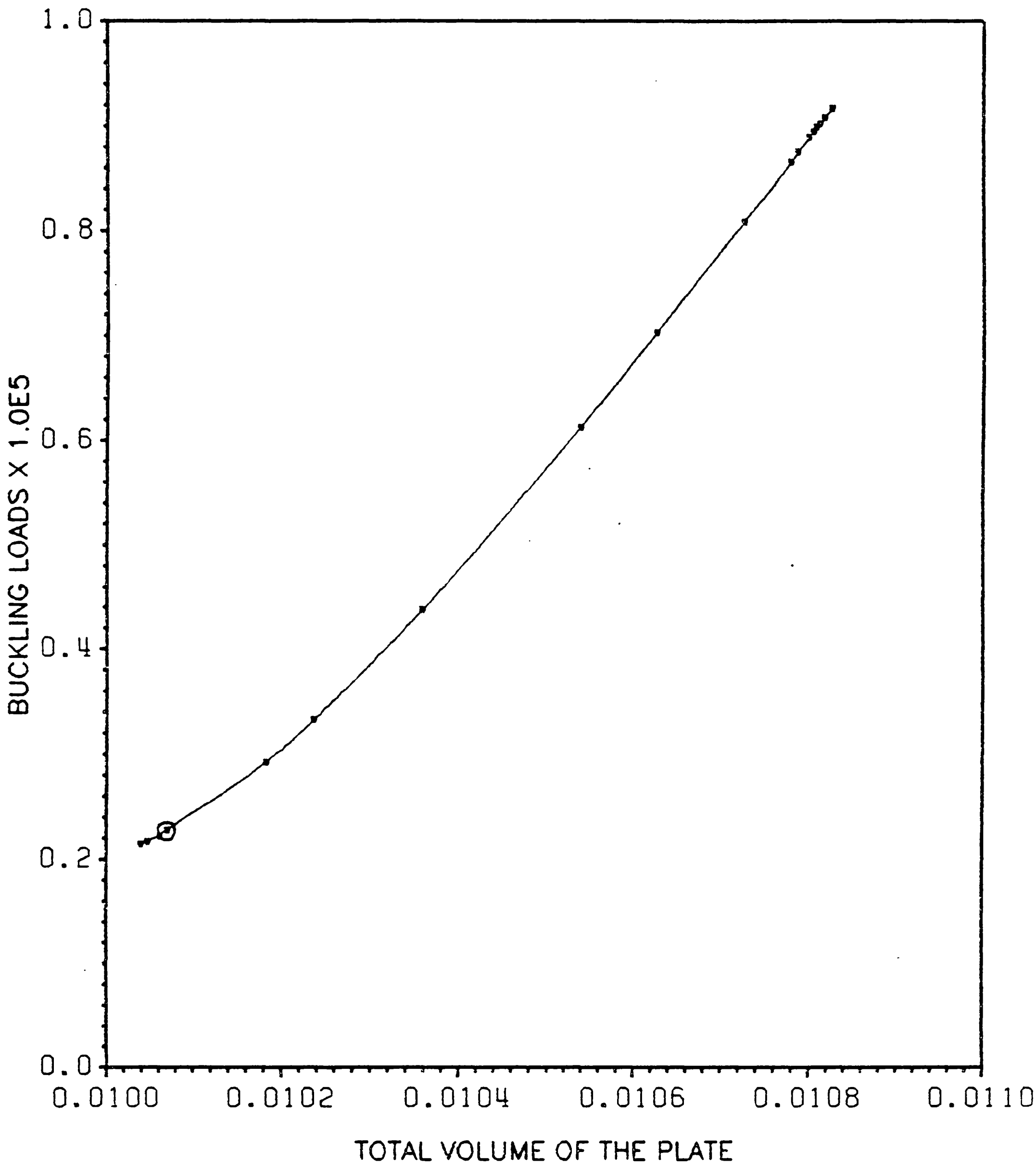

Figure 24. Nondimensional Buckling Loads for Optimum $(0°/90°/45°)_s$ stiffened laminates

Chapter 6

Concluding Remarks

Direct solution of optimality conditions was proposed in this study. It was shown that the optimality conditions which are obtained from variational formulation can be solved effectively using standard methods for nonlinear system of equations.

First, we employed a Newton-type method. A typical difficulty with the solution of optimality conditions is that there are many nonoptimal solutions. The use of second-order conditions was explored to validate solutions obtained from the first-order optimality conditions. Another difficulty in using a Newton-type method is that the method is not guaranteed to converge to the solution, unless the initial estimate is very close to the solution. A tracing technique was developed to eliminate this difficulty. The technique employs a homotopy method to trace the optimal solution with guaranteed convergence. In the present study, the original globally convergent homotopy method is adapted to the optimal structural design. The homotopy method showed definite advantage in the sense that we obtained an entire family of optima parameterized by the amount of resources. The solution path has several branches due to changes in the active constraint set. The Lagrange multipliers and second-order optimality conditions were used to detect branching points and to switch to the optimum solution path. The procedure was applied to find optimal foundation designs and optimal laminated plate designs.

This study reveals that the design problems with a buckling load constraint require very accurate nonlinear analysis because eigenvalues are placed quite closely as the design approaches to the optimum design. The bimodal formulation was given and it showed strong confidences in finding bimodal solutions. However, difficulty in tracing optimal solutions near trimodal design was experienced. The difficulty comes out from ill-conditioning of the Jacobian matrix in the homotopy tracing. Detailed studies on different formulations in relation to the condition of the Jacobian matrix are recommended for future work.

References

1. Dennis, J. E., Jr. and Schnabel, R. B., Numerical Methods for Unconstrained Optimization and Nonlinear Equations, Prentice-Hall, Englewood Cliffs, 1983.

2. Fox, R. L. and Schmit, L. A., "Advances in the Integrated Approach to Structural Synthesis," Journal of Spacecraft and Rockets, Vol. 3, 1966, pp. 858-866.

3. Fox, R. L. and Schmit, L. A., "An Integrated Approach to Structural Synthesis and Analysis," AIAA Journal, Vol. 3, 1965, pp. 1104-1112.

4. Fox, R. L. and Stanton, E. L., "Developments in Structural Analysis by Direct Energy Minimization," AIAA Journal, Vol. 6, 1968, pp. 1036-1042.

5. Haftka, R. T., "Simultaneous Analysis and Design," AIAA Journal, Vol. 23, No. 7, 1985, pp. 1099-1103.

6. Haftka, R. T. and Kamat, M. P., "Simultaneous Nonlinear Analysis and Design," presented at the ASME Design Automation Conference, Cincinnati, Ohio, Sept. 1985, to be published in Computational Mechanics, 1988.

7. Johnson, O. B., Micchelli, C. A., and Paul, G., "Polynomial preconditioners for conjugate gradient calculations," SIAM J., Vol. 20, 1983, pp. 362-376.

8. Hughes, T. J. R., Wingt, J., Levit, I., and Tezduyar, T. E., "New Alternating Direction Procedures in Finite Element Analysis Based on EBE Approximate Factorization," Computer Methods for Nonlinear Solid and Structural Mechanics, (S. Atluri and N. Perrone, editors), AMD, Vol. 54, 1983, pp. 75-109.

9. Watson, L. T., "A globally convergent algorithm for computing fixed points of C^2 maps," Appl. Math. Comput., Vol. 5, 1979, 297-311.

10. Watson, L. T., "Fixed points of C^2 maps," J. Comp. Appl. Math., Vol. 5, 1979, 131-140.

11. Watson, L. T., "Solving the nonlinear complementarity problem by a homotopy method," SIAM J. Control Optim., Vol. 17, 1979, 36-46.

12. Watson, L. T., "An algorithm that is globally convergent with probability one for a class of nonlinear two-point boundary value problems," SIAM J. Numer. Anal., Vol. 16, 1979, 394-401.

13. Wang, C. Y. and Watson, L. T., "Viscous flow between rotating disks with injection on the porous disk," Z. Angew. Math. Phys., Vol. 30, 1979, 773-787.

14. Watson, L. T., "Numerical study of porous channel flow in a rotating system by a homotopy method," J. Comp. Appl. Math., Vol. 7, 1981, 21-26.

15. Wang, C. Y. and Watson, L. T., "On the large deformations of C-shaped springs," Int. J. Mech. Sci., Vol. 22, 1980, 395-400.

16. Watson, L. T., Holzer, S. M., and Hansen, M. C., "Tracking nonlinear equilibrium paths by a homotopy method," Nonlinear Anal., Vol. 7, 1983, 1271-1288.

17. Watson, L. T. and Yang, W. H., "Optimal design by a homotopy method," Applicable Anal., Vol. 10, 1980, 275-284.

18. Watson, L. T. and Yang, W. H., "Methods for optimal engineering design problems based on globally convergent methods," Comput. and Structures, Vol. 13, 1981, 115-119.

19. Kiusalaas, J., "Optimal Design of Structures with Buckling Constraints," International Journal of Solids and Structures, Vol. 9, 1973, pp. 863-878.

20. Kamat, M. P. and Simitses, G. J., "Optimal Beam Frequencies by the Finite Element Displacement Method," International Journal of Solids and Structures, Vol. 9, 1973, pp. 415-429.

21. Adali, S., "The Design of Beams on Winkler-Pasternak Foundations for Minimum Dynamic Response and Maximum Eigenfrequency," Journal de Mecanique Theorique et Appliquee, Vol. 1, 1982, pp. 975-993.

22. Turner, H. K. and Plaut, R. H., "Optimal Design for Stability Under Multiple Loads," Journal of the Engineering Mechanics Division, ASCE, Vol. 106, 1980, pp. 1365-1382.

23. Gajewski, A., "Bimodal Optimization of a Column in an Elastic Medium, with Respect to Buckling or Vibration," International Journal of Mechanical Sciences, Vol. 27, 1985, pp. 45-53.

24. Plaut, R. H., Johnson, L. W., and Olhoff, N., "Bimodal Optimization of Compressed Columns on Elastic Foundations," Journal of Applied Mechanics, Vol. 53, 1986, pp. 130-134.

25. Szelag, D. and Mroz, Z., "Optimal Design of Vibrating Beams with Unspecified Support Reactions," Computer Methods in Applied Mechanics and Engineering, Vol. 19, 1979, pp. 333-349.

26. Haug, E. J. and Arora, J. S., Applied Optimal Design, Wiley, New York, 1979, p. 60.

27. Powell, M. J. D., "A Hybrid Method for Nonlinear Equations," Numerical Methods for Nonlinear Algebraic Equations, P. Rabinowitz, editor, Gordon and Breach, London, 1970.

28. Hetenyi, M., Beam on Elastic Foundation, The University of Michigan Press, Ann Arbor, 1946.

29. Riks, E., "An incremental approach to the solution of snapping and buckling problems," Int. J. Solids Structures, Vol. 15, 1979, 529-551.

30. Wempner, G. A., "Discrete approximations related to nonlinear theories of solids," Int. J. Solids Structures, Vol. 7, 1971, 1581-1599.

31. Crisfield, M. A., "A fast incremental/iterative solution procedure that handles 'snap-through'," Computers and Structures, Vol. 13, 1981, 55-62.

32. Watson, L. T., "Numerical linear algebra aspects of globally convergent homotopy methods," SIAM Review, Vol. 28, 1986, 529-545.

33. Chao, C. C., Koh, S. L., and Sun, C. T., "Optimization of Buckling and Yield Strengths of Laminated Composites," AIAA Journal, Vol 13, 1975, 1131-1132.

34. Chen, T. L. C. and Bert, C. W., "Design of Composite-Material Plates for Maximum Uniaxial Compressive Buckling," Proc. Oklahoma Academy of Science, Vol. 56, 1976, 104-107.

35. Bert, C. W., "Optimal Design of Composite-Material Panels for Business Aircraft," Business Aircraft Meeting of Society of Automotive Engineers, Wichita, Kansas, March 29 - April 1, 1977.

36. Bert, C. W., "Optimal Design of Composite-Material Plate to Maximize its Fundamental Frequency," Journal of Sound and Vibration, Vol. 50, 1977, 229-237.

37. Bert, C. W., "Design of Clamped Composite Plates to Maximize Fundamental Frequency," Journal of Mechanical Design, Vol. 100, 1978, 274-278.

38. Hirano, Y., "Optimum Design of Laminated Plates Under Axial Compression," AIAA Journal, Vol. 17, 1979, 1017-1019.

39. Tauchert, T. R. and Adibhatla, S., "Design of Laminated Plates for Maximum Stiffness," Journal of Composite Materials, Vol. 18, 1984, 58-69.

40. Tauchert, T. R. and Adibhatla, S., "Design of Laminated Plates for Maximum Bending Strength," Engineering Optimization, Vol. 8, 1985, 253-263.

41. Adali, S., "Optimization of Fibre Reinforced Composite Laminates Subject to Fatigue Loading," Proc. of 3rd Int. Conf. on Composite Structures, 9-11 Sept. 1985, Scotland.

42. Pedersen, P., "Minimum Flexibility of Non-Harmonic Loaded Laminated Plates," in Mechanical Characterization of Fibre Composite Materials, ed. R. Pyrz, Aalborg University, Denmark, 1986, 182-196.

43. Lukoshevichyus, R. S., "Minimizing the Mass of Reinforced Rectangular Plates Compressed in Two Directions in a Manner Conducive Toward Stability," Polymer Mechanics, Vol. 12, 1976, 929-933.

44. Schmit, L. A., Jr. and Farshi, B., "Optimum Design of Laminated Fibre Composite Plates," International Journal for Numerical Methods in Engineering, Vol. 11, 1977, 623-640.

45. Starnes, J. H., Jr. and Haftka, R. T., "Preliminary Design of Composite Wings for Buckling, Strength, and Displacement Constraints," Journal of Aircraft, Vol. 16, 1978, 564-570.

46. Rao, S. S. and Singh, K., "Optimum Design of Laminates with Natural Frequency Constraints," Journal of Sound and Vibration, Vol. 67, 1979, 101-112.

47. Anderson, M. S., Stroud, W. J, Durling, B. J., and Hennessy, K. W., "PASCO: Structural Panel Analysis and Sizing Code Users Manual," NASA TM-80182, 1981.

48. Bushnell, D, "PANDA2 - Program for Minimum Weight Design of Stiffened Composite Locally Buckled Panels," Lockheed Palo Alto Research Laboratory, Palo Alto, CA, LMSC-D06775, July, 1986.

49. Mesquita, L. and Kamat, M. P., "Structural Optimization for Control of Stiffened Laminated Composite Using Nonlinear Mixed Integer Programming," Virginia Polytechnic Institute and State University Report, No. VPI-E-85-26, 1985.

50. Mesquita, L. and Kamat, M. P., "Structural Optimization for Control of Stiffened Laminated Composite Structures," Journal of Sound and Vibration, Vol. 116, 1987, 33-48.

51. Olson, G. R. and Vanderplaats, G. N., "A Method for Nonlinear Optimization with Discrete Design Variables," Proceedings of the AIAA/ASME/ASCE/AHS Structures, Structural Dynamics and Materials Conference, Monterey, California, Vol. 1, April, 1987, 343-350.

52. Bogner, F. K., Fox, R. L., and Schmit, L. A., Jr., "The Generation of Interelement-Compatible Stiffness and Mass Matrices by the Use of Interpolation Formulas," Proc. Conf. Matrix Methods Struct. Mech., Wright-Patterson Air Force Base, Ohio, 1965, AFFDL TR 66-80, 1966.

53. Scott, D. S. and Parlett, B. N., "LASO2," NETLIB, Argonne National Lab., Argonne, IL, 1983.

54. Golub, G. H., Underwood, R., and Wilkinson, J. H., "The Lanczos Algorithm for the Symmetric $Ax = \lambda Bx$ Problem," Report STAN-CS-72-270, Department of Computer Science, Stanford University, Stanford, Calif., 1972.

55. Thielemann, W., "Contribution to the Problem of Buckling of Orthotropic Plates with Special Reference to Plywood," Report NACA.TM.1263, 1950.

The vita has been removed from the scanned document